MDPI

Review

Metal-Air Batteries—A Review

Abdul Ghani Olabi [1,2]**, Enas Taha Sayed** [3,4]**, Tabbi Wilberforce** [2]**, Aisha Jamal** [1]**, Abdul Hai Alami** [1]**,
Khaled Elsaid** [5]**, Shek Mohammod Atique Rahman** [1]**, Sheikh Khaleduzzaman Shah** [6,*]
and Mohammad Ali Abdelkareem [1,3,4,*]

[1] Department of Sustainable and Renewable Energy Engineering, University of Sharjah,
Sharjah P.O. Box 27272, United Arab Emirates; aolabi@sharjah.ac.ae (A.G.O.);
U16104495@sharjah.ac.ae (A.J.); aalalami@sharjah.ac.ae (A.H.A.); srahman@sharjah.ac.ae (S.M.A.R.)

[2] Mechanical Engineering and Design, School of Engineering and Applied Science, Aston University,
Aston'Triangle, Birmingham B4 7ET, UK; t.awotwe@aston.ac.uk

[3] Center for Advanced Materials Research, University of Sharjah, Sharjah P.O. Box 27272, United Arab Emirates;
e.kasem@mu.edu.eg

[4] Chemical Engineering Department, Minia University, Elminia 61519, Egypt

[5] Chemical Engineering Program, Texas A&M University at Qatar, Doha 23874, Qatar;
khaled.elsaid@qatar.tamu.edu

[6] Renewable Energy and Energy Efficiency Group, Department of Infrastructure Engineering,
Melbourne School of Engineering, The University of Melbourne, Melbourne, VIC 3010, Australia

[*] Correspondence: sheikhkhaleduzzaman.shah@unimelb.edu.au (S.K.S.);
mabdulkareem@sharjah.ac.ae (M.A.A.)

Abstract: Metal–air batteries are a promising technology that could be used in several applications, from portable devices to large-scale energy storage applications. This work is a comprehensive review of the recent progress made in metal-air batteries MABs. It covers the theoretical considerations and mechanisms of MABs, electrochemical performance, and the progress made in the development of different structures of MABs. The operational concepts and recent developments in MABs are thoroughly discussed, with a particular focus on innovative materials design and cell structures. The classical research on traditional MABs was chosen and contrasted with metal–air flow systems, demonstrating the merits associated with the latter in terms of achieving higher energy density and efficiency, along with stability. Furthermore, the recent applications of MABs were discussed. Finally, a broad overview of challenges/opportunities and potential directions for commercializing this technology is carefully discussed. The primary focus of this investigation is to present a concise summary and to establish future directions in the development of MABs from traditional static to advanced flow technologies. A systematic analysis of this subject from a material and chemistry standpoint is presented as well.

Keywords: metal-air battery; metal–air flow batteries; cell design; applications; challenges

1. Introduction

Researchers and politicians are becoming increasingly focused on energy storage as the awareness of the environmental implications that come with relying on fossil commodities and the reliability and long-term durability of electricity networks increases across the globe. Energy storage can assist in resolving the issue of intermittency associated with wind and solar power; in some cases, this can react quickly to substantial demand changes, allowing the grid to respond more rapidly and reducing the need to implement backup power plants. Energy storage is becoming increasingly popular. The efficiency of an energy storage facility is defined by the speed with which it can react to changes in demand, the total amount of energy it can store, the rate at which energy is lost throughout the storage process, and the ease with which it can be recharged. Solar PV only provides electricity during the day, at its most productive. Every day brings a new level of total output. Wind energy output is erratic, yet it may be spread around the world. On the other hand, average

performance may vary significantly; for example, in one area of Germany alone, there can be an almost 20 GW difference in performance over the course of a day [1]. Because of the intermittent development of renewable energy, it is difficult to maintain a stable equilibrium in terms of supply and demand. The shutdown of traditional power facilities reduces the capacity to regulate frequency, and so energy storage is necessary. Energy storage may also be used to meet the demand for energy at peak periods, such as when air conditioners are turned on in the summer or when homes switch on lights and appliances in the evening. Electricity becomes more expensive when power plants are forced to boost output to satisfy the increasing demand for energy during peak hours. Energy storage improves grid efficiency by allowing utilities to buy power during off-peak hours when energy is cheaper and sell it back to the grid when energy is more in demand [2–4], thus increasing system efficiency.

Among the different available energy storage devices, batteries have several advantages, such as high efficiency, and are available in different sizes [5]. The evolution of batteries can be traced back to the 1800s when physicist Alessandro Volta conceptualized the development of this technology. A battery is a device that is functional via electrochemical reactions in a cell or several cells connected in series [6,7]. The primary function of a battery is to store power via an electrochemical medium [8]. The three main components of the electrochemical cell are: an anode, a negative electrode (Reducing electrode where oxidation happens); a cathode, a positive electrode (Oxidizing electrode where reduction happens); and an electrolyte [9], which facilitates ion transfer between the two electrodes. An oxidation reaction, i.e., electron loss, occurs on the anodic electrode. The released electrons, having gained excitation, become mobile and flow via a circuit to the cathodic electrode, where reduction occurs. On the other hand, the charges flow freely between the electrodes of the battery via the electrolyte [10]. Batteries are subdivided into primary and secondary batteries. Non-rechargeable batteries, often called primary batteries, are designed not to be recharged once they discharge energy [11]. However, it has been reported [12,13] that these batteries are tiny, light, cheap, and straightforward sources of electricity that are appropriate for a wide range of portable equipment. On the other hand, a secondary battery is rechargeable, since it may be electrically recharged after it has been discharged [14,15]. This is because secondary batteries operate based on the reversible redox reactions, and the reversible reactions realize the charge-discharge functions. Secondary batteries, such as lithium-ion, lead-acid, zinc-air, nickel-cadmium, etc., can be recharged several times. The following table (Table 1) summarises the crucial aspects of the common types, i.e., Li-ion, lead-acid, and redox flow batteries.

Metal-air batteries (MABs) are one kind of battery that is both safer and has a higher energy density than other types. The utilization of oxygen from ambient air as a cathode source has the additional benefit of lowering the cost and weight of the MAB considerably. Furthermore, the anode of the MAB may be constructed from low-cost materials [16].

Table 1. The mean features of the common batteries, i.e., Li-ion, lead-acid, and redox flow batteries.

Battery Type	Power	Energy Density (Wh/Kg)	Operating Voltage (V)	Discharge Time, h	Cost ($/kWh)	Life Time at 80% DoD * Cycles	Main Advantage	Main Disadvantage	Energy Efficiency %	Ref.
Li–ion	1 kW–1 MW	100–200 (150–200 Wh/L)	3.6–4	0.1–10	800 (2006) 268 (2015)	4500–8000	High energy	Poor safety	93	[17–19]
Lead–acid	1 kW–10 MW	20–40 (50–70 Wh/L)	2.1	0.01–1	150	200–2000	Low cost	Short life cycle	85	[17,19, 20]
Redox flow	100 kW–80/90 MW	2–32 (25–30 Wh/L)	1.4	1–10	223	2000–4000	Flexible design	Low energy density	82	[2,21,22]

* Dod: depth of discharge.

An electrolyte (aqueous or non-aqueous) and a bi-functional air electrode are the primary components of a metal-air battery. Metal electrodes include zinc, lithium, magnesium, aluminum, and other metals. This device's fundamental working concept is to

electrochemically reduce O_2 from the air and oxidize the metal electrode, resulting in the formation of solid metal oxides that may be recycled. Compared to Li-ion systems, this method allows for substantial reductions in both the volume and weight of the battery. The theoretical energy density and specific energy of metal-air systems are shown in Figure 1, which provides a comparison of these values.
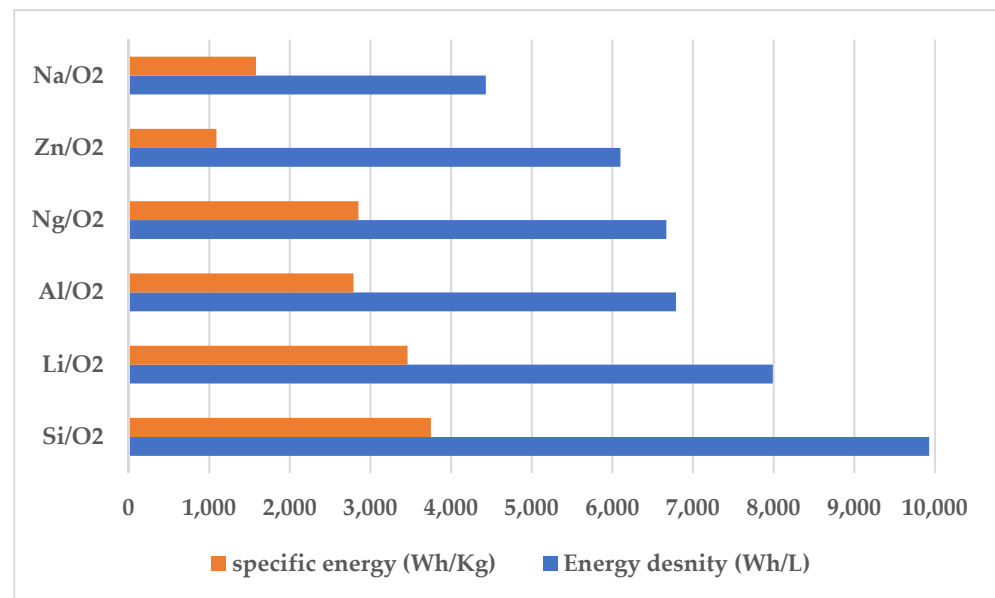

Figure 1. Theoretical energy density and specific energy (including oxygen) of commonly researched metal-air batteries [23].

It has been shown that in certain non-ideal situations, the precipitation of the solid discharge product may consume active electrolyte components, lowering the energy density that can be achieved [24]. The investigation of a wide range of metal-air chemistries is continuing. Mg-air systems are attractive because of the uniform deposition of Mg metal [25–27], but the corrosion of the Mg electrode severely restricts aqueous Mg-air batteries. Several ionic liquid electrolytes have been suggested for use in magnesium-air systems. Still, they all suffer from electrochemical instability [28], especially noticeable during charging, and the cell's reversibility is restricted. Al-air is another intriguing candidate to consider. As an available and safe element, aluminum is used in the production of Al-air batteries, which provide both a high theoretical energy density and high specific energy values [29–31]. A combination of sodium's abundant natural supply and safety, as well as its characteristics that are similar to lithium, has fueled research into Na-air batteries [32–34]. The development of these systems is still in its stage. Si-air batteries have also received a lot of attention recently [35]. They have a high theoretical energy density and are stable in electrolytes, including aqueous solutions. However, the reversibility of the solid discharge product, precipitation, and pore blockage are all issues that are presently being addressed in experimental investigations of Si-air systems in both ionic liquid and alkaline electrolytes. Li-air and Zn-air are two of the most promising metal-air systems now under study [36,37], with Li-air being the most promising. Lithium-air batteries (LABs) have been studied for decades [38], but they have only recently emerged as a highly explored subject in the scientific community. The electrolyte has proven to be a stumbling block in the advancement of LAB technology. The aprotic (non-aqueous) and aqueous electrolyte combinations used in Li-air systems are the most often seen. The use of mixed electrolyte systems has been suggested. The first wave of LAB investigation concentrated on aprotic electrolytes, which was the start of the wave. Using the aprotic Li-air system (LiPF6 in ethylene carbonate (EC)), Abraham et al. [39] suggested an overall reaction resulting in the formation of Li_2O_2 or Li_2O, which was published in 1996. Carbonate

solvents were used in the first generation of aprotic Li-air cells; however, it has subsequently been shown that carbonate solvents are unstable, releasing lithium carbonates during discharging and emitting CO_2 during charging [40]. In recent years, carbonate electrolytes have mostly been phased out in favor of ether and ester solvents in conjunction with lithium salts. The precipitation of Li_2O_2 poses a second difficulty for LABs in aprotic electrolytes, which presents the third obstacle. When this solid precipitates in the cathode, it may create a thick layer over the carbon surface, preventing electrons from transferring between it and the anode. It is possible that whole pores in the cathode may become closed as precipitation proceeds, resulting in the electrode being passivated and reducing the cell's capacity. Finally, it has been shown that oxygen transport in aprotic electrolytes may be a difficult component to control in LAB effectiveness, particularly at higher current densities [41]. This has prompted researchers to draw lessons from the success of the gas diffusion electrode in fuel cells and to continue studies of LABs using aqueous electrolytes as an alternative. It is widely known that Li metal interacts strongly with water, which has traditionally restricted aqueous electrolytes in Li-air systems. However, the usage of aqueous electrolytes has recently been expanded. When a glass-ceramic layer over the Li electrode was successfully suggested in 2004, it allowed for the electrochemical process to continue while also protecting the metal electrode [42]. In alkaline aqueous electrolytes, the discharge product is LiOH H_2O rather than Li_2O_2, indicating that the electrolyte is alkaline. These systems allow for LiOH to precipitate at the separator–anode interface, which lowers the danger of pore-clogging in the cathode, which has been seen in aprotic laboratory systems. While in the presence of air, dissolved CO_2 interacts with OH^- to create carbonates, which gradually decreases the conductivity of the electrolyte and shortens its lifespan. When exposed to water, dissolved CO_2 reacts with OH– to form carbonates, which further shortens the cell's lifetime. Many theoretical studies have highlighted the impressive possibilities of these systems [42], and the company International Business Machines (IBM) has sought the expansion of LABs for industrial purposes. IBM has also pursued the growth of LABs for commercial applications. Even though there are still major difficulties [43,44], the future of LABs seems bright. Zinc-air batteries (ZABs) are the only completely developed metal–air system now available, and they have been successfully marketed as primary cells for many decades. Hearing aids, for example, are a low-current application that they are particularly suited for. Their lifespan and electrical rechargeability, on the other hand, are both limited [45]. One significant benefit of Zn as an electrode material is that it is stable in water, unlike Li, which is a significant advantage. Alternate near-neutral aqueous [46] and ionic liquid electrolytes have been suggested in an attempt to enhance the rechargeability of ZABs. Current research continues to be focused on material development to overcome the lifespan limits of these systems and cell engineering to enhance the effectiveness of the system. However, although some obstacles persist, the advancement of secondary ZABs has progressed to the point where they may be feasible for stationary storage applications. Some start-ups, such as Eos Energy Storage and Fluidic Energy [47], are working to commercialize the innovation. Zn-air systems provide one of the most rapid and dependable routes to today's practical secondary metal-air battery systems.

2. MABs' Theoretical Considerations and Mechanisms

As a result of the oxygen being kept outside the battery, MABs are a viable choice among several other types of energy storage devices. The oxygen-evolution reaction (OER) and the oxygen-reduction reaction (ORR) are the two processes related to oxygen. Generally speaking, MABs function in an open system [48]. The components are represented by the schematic design seen in Figure 2. This system comprises three basic parts: a metal anode, a porous air cathode, and an electrolyte that separates the two electrodes from one another. As implied by the name, the anode material of a metal-air battery is composed of metals such as lithium Li, sodium Na, iron Fe, zinc Zn, and other elements. There are many types of electrolytes available [49]. They include: aqueous electrolytes, non-aqueous

(aprotic), solid-state, and hybrid electrolytes. Because of their extraordinary sensitivity to water, lithium-air, potassium-air, and sodium-air batteries were often used in non-aqueous systems. While anodes composed of magnesium, aluminum, iron, or zinc are compatible with aqueous electrolytes, these aqueous systems need the addition of a hydrophobic protective layer to prevent electrolyte leakage [48].
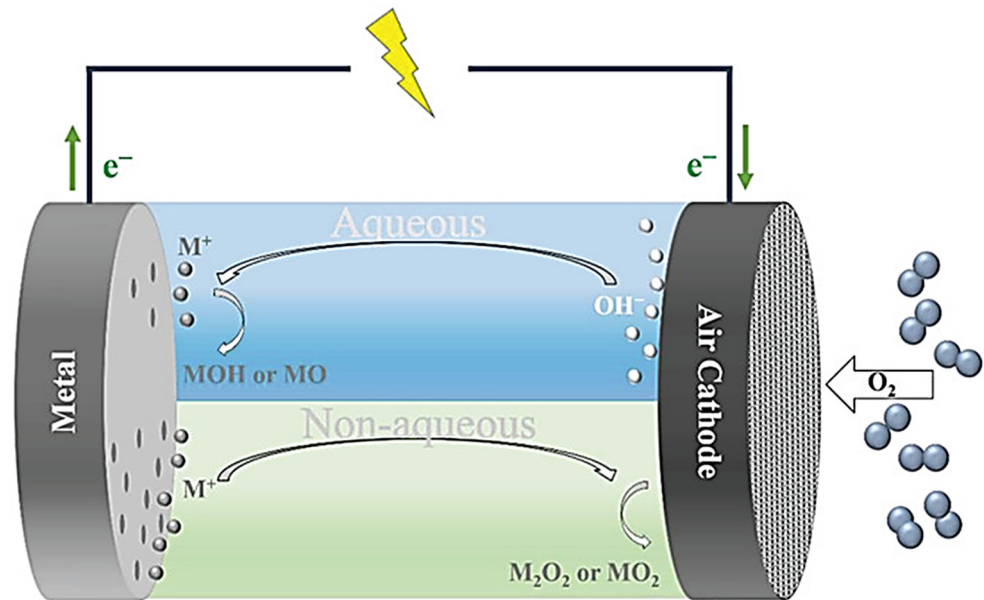

Figure 2. Diagram of metal-air batteries, adapted from [50].

In MABs, metal changes into ions on the anodic electrode, while the oxygen transforms into hydroxide ions at the cathodic electrode. This is in contrast to the operating approach of a conventional ionic battery, which sees metallic ions transition from the anode to cathode. The diffusion of oxygen into the MAB occurs via a layer known as the gas diffusion layer. The behavior of oxygen in an aqueous electrolyte medium differs from that of oxygen in a non-aqueous electrolyte, as depicted in Figure 3.
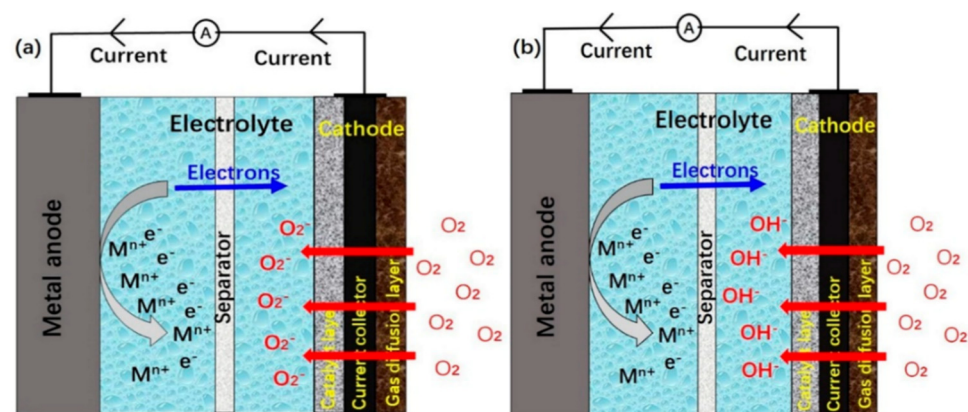

Figure 3. MABs' operational characteristics in (**a**) non-aqueous and (**b**) aqueous electrolyte, adapted from [16].

During the transition of the metal into metallic ions, electrons are produced, and the metallic ions subsequently dissolve into the electrolyte. During a charging operation, all of these steps are reversed. The reaction formulae for several MABs are shown in Table 2.

Table 2. Cathode, anode, and overall reactions of metal–air batteries.

Metal Anode	Electrolyte	Anode Reaction	Cathode Reaction	Overall Reaction	Ref.
General		$M \rightleftarrows M^{n+} + ne^-$	$O_2 + 2H_2O + 4e^- \rightleftarrows 4OH^-$		[16]
Iron Fe	Alkaline aqueous	$Fe + 2OH^- \rightleftarrows$ $Fe(OH)_2 + 2e^-$ $3Fe(OH)_2 + 2OH^- \rightleftarrows$ $Fe_3O_4 + 4H_2O + 2e^-$	$O_2 + 2H_2O + 4e^- \rightleftarrows 4OH^-$	$2O_2 + 3Fe \rightleftarrows$ Fe_3O_4	[51]
Aluminum Al		$Al + 4OH^- \rightleftarrows$ $Al(OH)\ 4 - +3e^-$		$3O_2 + 2Al \rightleftarrows$ Al_2O_3	[32]
Zinc Zn		$Zn + 4OH^- \rightleftarrows$ $Zn(OH)_4^{2-} + 2e^-$ $Zn(OH)_4^{2-} \rightleftarrows$ $ZnO + 2OH^- + H_2O$		$O_2 + Zn \rightleftarrows ZnO$	[52]
Lithium Li	Non-aqueous	$Li \rightleftarrows Li^+ + e^-$	$O_2 + e^- \rightleftarrows O_2^-$ $O_2^- + Li^+ \rightleftarrows LiO_2$ $LiO_2 + Li^+ + e^- \rightleftarrows Li_2O_2$	$O_2 + Li \rightleftarrows Li_2O_2$	[53]

2.1. Cell Potential

The cell potential is determined by calculating the potential difference between the anodic and cathodic electrodes, as shown in the following equation [54,55]. The resulting value is expressed as a volt unit (V), as shown in Equation (1).

$$E^o_{cell} = E^o_{Red,Cathode} - E^o_{Red,Aonde} \ (1\,\text{M and 1 bar}) \tag{1}$$

If the standard circumstances are altered, the Nernst equation may be used as a guideline to calculate:

$$E = E^o - \frac{RT}{nF}lnQ \tag{2}$$

which is derived from Gibbs free energy

$$\Delta G^\circ = -nFE^\circ = \Delta H^\circ - T\Delta S^\circ \tag{3}$$

This is calculated using the balanced reaction equation and thermodynamic tables. When ΔG is a positive value, it implies the reaction requires external energy (nonspontaneous reaction), while when it is a negative value, the reaction can occur in the absence of external energy (spontaneous reaction) [54–56].

2.2. Energy Efficiency

The energy efficiency of a rechargeable battery is subdivided into three parts. First, the charging energy efficiency η_{charg}, which is equal to the net energy ΔQ_n divided by charge energy Q_{in} , as calculated as follows

$$\eta_{charg} = \frac{\Delta Q_n}{Q_{in}} \tag{4}$$

$$Q_{in} = \int_{SOC(0)}^{SOC(t)} U_{charge}C_n dSOC \tag{5}$$

$$\Delta Q_n = \int_{SOC(0)}^{SOC(t)} U_{OCV}C_n dSOC \tag{6}$$

$$SOC(t) = SOC(0) - \frac{\int Idt}{C_n} \ (I \text{ is positive when discharging the battery}) \tag{7}$$

which *SOC* refers to the state of charge, U is the battery voltage and C_n is the battery standard capacity. Secondly, the discharging energy efficiency;

$$\eta_{disch} = \frac{Q_{out}}{\Delta Q_n} \tag{8}$$

where the discharge energy is

$$Q_{out} = \int_{SOC(0)}^{SOC(t)} U_{disch} C_n dSOC \tag{9}$$

Finally, the charge-discharge energy efficiency is given as

$$\eta_{battery} = \frac{Q_{out}}{Q_{in}} \tag{10}$$

The charge energy Q_{in} and discharge energy Q_{out} can be calculated from the automatically recording data of the voltage, current, and time [57].

3. Electrochemical Performance of MABs

From the results of many tests, many kinds of metal utilized in MABs, such as Zn-air, Fe-air, Al-air/Al-O$_2$, Li-air/Li-O$_2$, and Si-air batteries, may offer medium-specific power and good specific energy. Additionally, as depicted in Figure 3, the prospective efficiency of MABs was contrasted with that of Li-ion (LIB) as well as metal-sulfur batteries. The specific energy supplied by prospective MABs, advanced metal-S batteries, and LIBs ranges from 500 to 1500 Wh/kg Me, up to 500 Wh/kg, and 200 to 300 Wh/kg, respectively, in terms of specific energy. While the specific power provided by prospective MABs, advanced metal–S batteries, and LIBs range from 0.1–1 kW/kg Me, up to 1 kW/kg, as well as up to 10 kW/kg. The specific power delivered by MABs, advanced metal–S batteries, and LIBs ranges from 0.1–1 kW/kg Me. The numbers on the right-hand side of Figure 4 reflect the possible future effectiveness of certain MABs [58], which are not yet available.
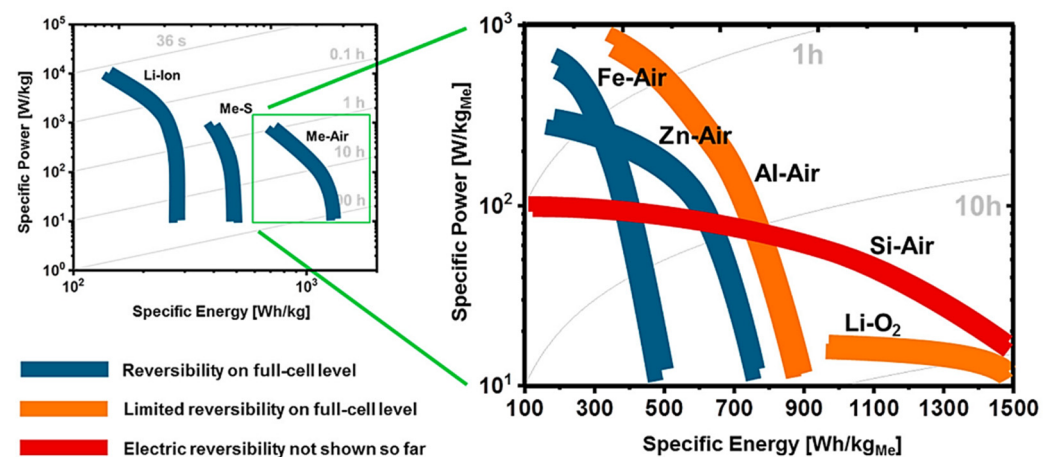

Figure 4. Ragone diagram for various types of batteries, adapted from [58].

Although a Li-air battery showed a high OCV of 2.91 V and high theoretical energy density, its lifetime was short, as it failed after two cycles due to the corrosion of the lithium anode by the electrolyte. A Na–air battery fabricated using a 3D tin sulfide nano-petals cathode showed a high round trip efficiency of 83%, a low overpotential gap of 0.52 V, good rechargeability (40 cycles), and a high power density of 300 W/kg [59]. The good performance was related to the 3D tin sulfide cathode that provides active sites for efficient diffusion of electrolyte and air [59]. An Al–air battery had an OCV of 1.2 V, the theoretical energy density of 2.98 Ah/g, and specific energy of 200 Wh/Kg [31]. The specific capacity

of an Al–air battery with a chitosan hydrogel membrane and 10% SiO_2 achieved a specific capacity of 288.5 mAh/g at 1 mA/cm^2 due to the generation of $SiO_3{}^{2-}$, which is considered a corrosion inhibitor [60]. Additionally, an Mg–air battery showed a specific energy density of 3.9 kWh/Kg and a theoretical volumetric density of 14 kWh/L [28]. Adding vanadate or phosphate as a corrosion inhibitor to the NaCl electrolyte significantly improved the performance of Mg-air batteries, and phosphate showed a stronger inhibiting effect than vanadate [61]. Zinc is a cheap and abundant metal; thus, the cost of ZABs is quite low. A Zn-air battery realized a theoretical energy density of 0.82 Ah/g. A Zn-air battery with Co-MOF as cathode catalyst achieved a power density of 86.2 mW/cm^2 and outstanding charge-discharge performance [62]. Additionally, a Zn–air battery with Ni_3Fe/N-S-CNT as the cathode electrocatalyst achieved 180 mW/cm^2 (power density) and long-term stability for 500 h [63]. A Fe-air battery had a specific charge capacity of 300 Ah/Kg, the theoretical open-circuit voltage of 1.28 V, charge efficiency of 96%, voltage efficiency of 40%, and energy efficiency of 35% [51]. A 3D-printed Fe-air battery with nanocomposite electrodes and showed a cell voltage of 0.76 V, the maximum charge capacity of 814 mA h/g at 10 mA/cm^2, and an energy density of 453 Wh/Kg [64]. The Sn–air battery is another type of metal-air battery, with an OCV of 0.95 V and 860 Wh/Kg specific energy. A Sn-air battery operated at room temperature with an electrolyte of methane sulfonic acid and polyacrylamide gel achieved a maximum power density of 5 mW/cm^2 at 12 mA/cm^2 for 24 h [65]. The following table (Table 3) summarizes the main differences between the reported MABs.

Table 3. Shows a comparison among the different available metal-air batteries.

Type	Calculated OCV (V)	Practical Energy Density (Wh/Kg)	Metal Cost ($/kg)	Efficiency (Discharge), %	Capacity Density (mA h/g)	Ref.
Fe/Air	1.28	50–75	0.4	96	300–786	[51]
Zn/Air	1.65	350–500	1.85	-	300–875	[52,66]
Mg/Air	2.93	400–700	2.75	-	737−2131	[28]
Al/Air	2.71	300–500	1.75	70	260–2777	[31,67,68]
Na/Air	2.27	1600	1.7	-	-	[69]
Li/Air	2.96	1700	68	68–94	3842	[70–73]
Sn/Air	0.95	-	21	70–90	-	[69,74]

4. Anode of MABs

Since the invention of the first metal-air battery, the zinc-air battery, in 1878, a great deal of development and study has been carried out, and Figure 5 displays a summary of some of these advancements [75]. Many metals, including zinc, aluminum, iron, lithium, sodium, potassium, and magnesium, may be used as anodes in MABs. Each metal has its own set of benefits and drawbacks when it comes to being used as anode electrodes. The energy density of LABs is the greatest theoretically possible (11,140 Wh/kg) among the many kinds of MABs; however, obtaining rechargeable LABs (LABs) is difficult. On the other hand, metals such as zinc (0.82 Ah g(−1)), magnesium (2.20 Ah g(−1)), as well as aluminum (Al) are ecologically benign, plentiful, commercially viable, as well as reasonably safe. Furthermore, Al is readily available for recycling in massive amounts, and it has a higher energy density (8.1 kWh·kg(−1)), as well as a significant theoretical voltage (2.7 V). As a result, AABs are considered to be the second most energy-dense battery after Li.

The chemical activity of the anode determines the discharge capacity of the anode. Because of the high activity of the metal, a side reaction with various components of the electrolyte may occur that cannot be avoided. These reactions may occur at different rates and have varying effects on battery efficiency, subject to the purity of metal and the storing conditions [28]. A list of theoretical specific energies for each kind of metal-air battery is provided in Table 4, with the specific energy computed using the following formula:

$$W_{Me/MeOx} = n \times F \times M_{Me/MeOx}{}^{-1} \times U_{cell} \qquad (11)$$

where W denotes the specific energy of the material, n denotes the number of atoms that have been transported, M denotes the molar mass, whilst U_{cell} is the cell voltage. Table 5 contains experimental findings [58], representing the most relevant results that have been published.
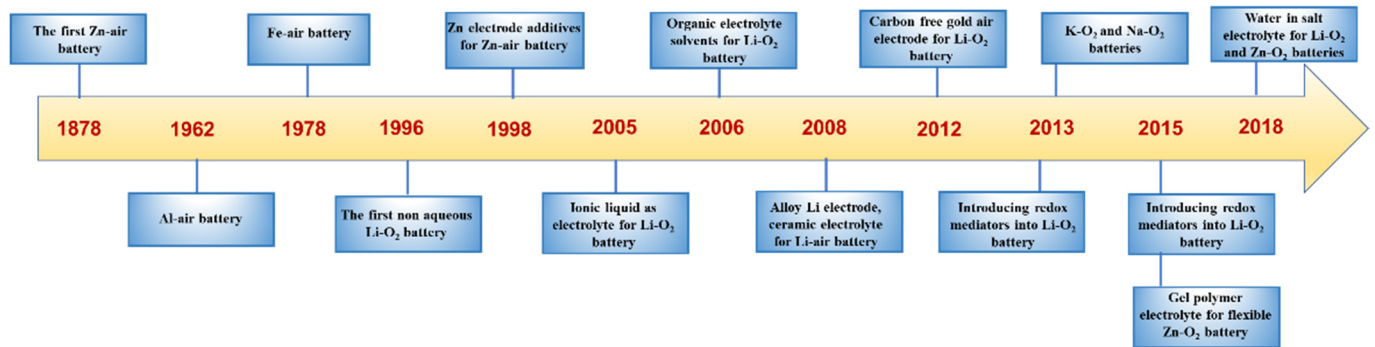

Figure 5. Research progress in MABs as a brief timeline. Reprint with permission [75]; Copyright 2019, Elsesiver.

Table 4. Various types of MABs have different theoretical specific energies.

| MAB | Energy $\left(\text{Wh kg}^{-1}\right)$ | | Voltage (V) | Electrolyte | Ref. |
	Including O_2	Without O_2 (Metal)			
Li/Air (Li$_2$O product)	5220	11,238	2.91	Non aqueous	[76,77]
Al/Air	2784	8091	2.7	Aqueous	[67]
	3311	6258	2.1	Non aqueous	[78]
Si/Air	3947	8461	2.21	Non aqueous	[79]
	2334	8001	2.09	Aqueous	[80]
Ca/Air (CaO product)	2996	4186	3.13	Non aqueous	[81]
Mg/Air	2848	6098	2.77	Aqueous	[58]
	3919	6493	2.95	Non aqueous	[82]
Na/Air (Na$_2$O$_2$ product)	1601	2716	2.33	Non aqueous	[83]
Fe/Air	764	1229	1.28	Aqueous	[84]
Zn/Air	1086	1352	1.65	Aqueous	[52]
K/Air	935	1700	2.48	Non aqueous	[85]
Sn/Air (at 1000 K)	860	6250	0.95	Non aqueous	[69]

Table 5. The recent experimental results of different MABs, adapted from [58].

MAB	Discharge Product	Experiment Specific Energy $\left(\text{Wh kg}^{-1}\right)$	Condition	Reversibility Cycles	Voltage (V) Ref.
Fe/O$_2$	Fe(OH)$_2$	453 Wh/kg$_{Fe}$	[b,c,d,e]	3500 [b,d]	1.28
Zn/O$_2$	ZnO	>700 Wh/kg$_{Zn}$	[a,c,d]	>75 [a,c]	1.65
K/O$_2$	KO$_2$	~19,500 Wh/kg$_{Carbon}$	[a,c,d]	>200 [a,c]	2.48
Na/O$_2$	Na$_2$O$_2$ NaO$_2$	~18,300 Wh/kg$_{carbon}$	[a,c,d]	>20 [a,c]	2.33 2.27
Mg/O$_2$	Mg(OH)$_2$ MgO	~2750 Wh/kg$_{cathode}$	[a,c,d,f]	<10 [a,c,d]	2.77 2.95
Si/O$_2$	Si(OH)$_4$ SiO$_2$	~1600 Wh/kg$_{Si}$	[a,c,d]	Not yet	2.09 2.21
Al/O$_2$	Al(OH)$_3$ Al$_2$O$_3$	~2300 Wh/kg$_{Al}$	[a,c,d]	Limited	2.71 2.1
Li/O$_2$	Li$_2$O$_2$ Li$_2$O	>11,050 Wh/kg$_{carbon}$	[a,c,d]	>250 [a,c]	2.96 2.91

Conditions: a is anode sheet/foil, b is porous/particulate anode, c is full-cell measurements, d is 100% deep discharge, e is repeated charge/discharge, and f is elevated temperature.

Progress Done in the Anode of MAB

As discussed above, several metals, such as zinc, aluminum, iron, lithium, sodium, potassium, and magnesium, can be used as anodes in MABs. Each metal has its advantages and disadvantages. The Al–air battery has unique features, such as high energy density, light weight, good recyclability, environmentally friendly, and cheap. Moreover, the electrolyte can be an alkaline, salty, and non-aqueous solution [86]. Therefore, we will focus in this section on the progress made in Al–air batteries.

The performance of an ultrafine-grain (UFG) aluminum anode produced by equal channel angular pressing (ECAP) (Figure 6) in three distinct electrolytes (NaOH, KOH, and NaCl) was studied at a constant discharge current of 10 mA cm^{-2}. The cathode was an air electrode with gas diffusion and catalyst (Ag powder) layers as a double-layer structure, laminated with a current collector (Ni mesh). The UFG was also compared with coarse-grained (CG) aluminum. The results shown in Table 6 indicate that the grain with finer sizes enhanced the battery's performance in alkaline electrolytes because of the active dissolution of the aluminum anode. However, due to the local corrosion and the oxide film blockage in NaCl electrolyte, the study results show that changing the Al anode grain to a fine size has no effect on performance. The anode efficiency of CG and UFG in NaOH is 55.3% and 77.4%, respectively. Moreover, the energy density improved by 55.5% with a finer grain size relative to CG, but the effect in NaCl and KOH solutions is not clear [87].
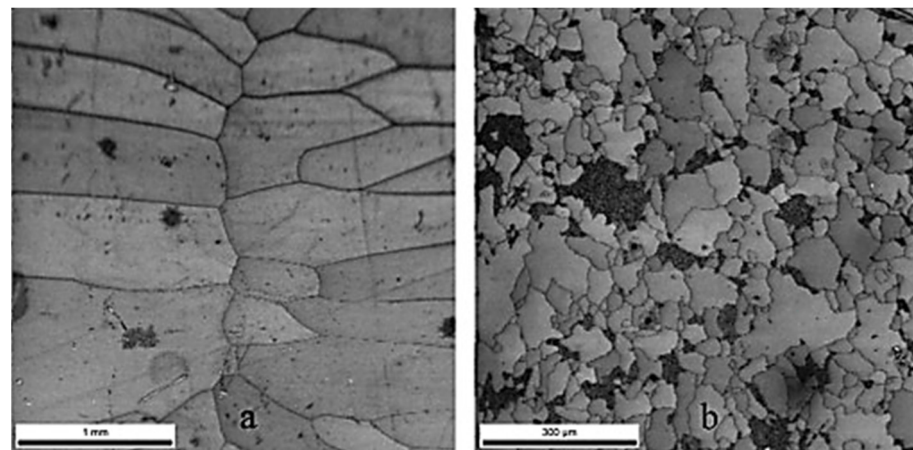

Figure 6. Micrograph of Al anode (**a**) cast and (**b**) equal channel angular pressing (ECAP). Reprint with permission [87]; Copyright 2019, EDP Sciences.

Table 6. The characteristic performance of Al–air battery using different Al anodes at a current density of 10 mAcm^{-2}, with permission to reproduce from [87].

Electrolyte Solution	Aluminum Anode	Average Discharge Voltage (v)	Capacity Density (Ah/kg)	Efficiency (%)	Energy Density (Wh/kg)
2 M NaCl	CG	0.398	2751	92.3	1097
	UFG	0.387	2726	91.6	958.4
4 M KOH	CG	1.38	2439	81.7	3363
	UFG	1.44	2475	83.1	3593
4 M NaOH	CG	1.397	1647	55.2	2428
	UFG	1.532	2307	77.3	3524

Two aluminum anodes with different purity percentages were compared to examine the impact of the impurity on the performance of the aluminum–air batteries. The tested anodes were a 2N5 purity 99.5% and a 4N purity 99.99% grade aluminum anode. The experimental results show that the 2N5 grade Al showed a lower battery performance than the 4N grade Al due to the impurities that shaped the complex layer containing iron,

silicon, cupper, and other elements. This impurity layer of 2N5 aluminum decreases the battery's voltage on standby status and depletes the battery efficiency and the discharge current at 1 volt; however, lower voltages of 0.8 volts lead to the layer dissolving, and thus the performance improved. The results at the two different applied potentials are shown in Table 7. We can conclude that the impurity complex layer reduced with a declining discharge voltage. This phenomenon improves battery efficiency and discharges current density by reducing the self-corrosion reaction. Therefore, it is possible to use the cheaper 2N5 grade aluminum anode instead of 4N Al at the condition of high-power discharge for aluminum-air batteries [88].

Table 7. Characteristics of 2N5 and 4N grade aluminum-air batteries at 1 and 0.8 V applied potentials, with permission to reproduce from [88].

Voltage (V)	Anode	Electric Capacity (C)	Electric Capacity/Discharge (C)	Performance (%)
1 V	4N grade Al	1467.23	751.30	50.92
	2N5 grade Al	1991.22	377.47	18
0.8 V	4N grade Al	2211.13	1590.70	71.76
	2N5 grade Al	2151.14	1625.61	75

Zinc is considered an effective alloying element for the anode of an aluminum-air battery to increase the nominal cell voltage and decrease the self-corrosion rate. However, a study found that Zn added to Al 99.7% purity anode decreased its discharge performance due to the formation of Zn oxidation film. Additionally, to overcome this formation, indium (In) was added to an aluminum-zinc anode, which showed improvement in the discharge performance of Al–air batteries by reducing the resistance of zinc oxidation film via In ions. Moreover, an Al-Zn-In alloy anode that is made of commercial-grade aluminum (99.7% purity) has a cheaper cost than 4N grade aluminum (99.99% purity) [89].

5. MABs Electrolyte

As depicted in Figure 7 [16], the electrolyte for MABs may be aqueous, non-aqueous, solid-state, or hybrid in nature. This section covers the recent progress made in the different electrolytes used in MABs.
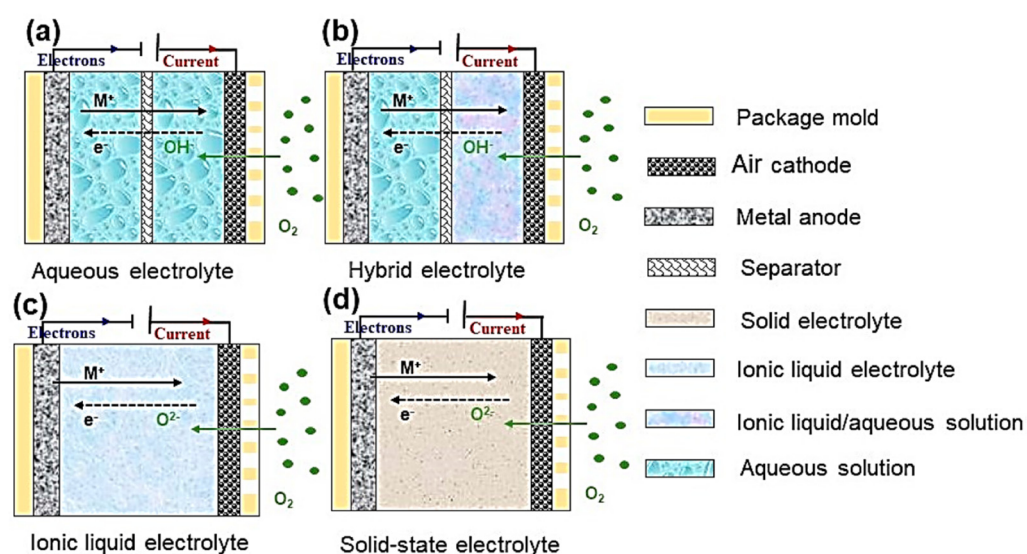

Figure 7. Different electrolytes of metal-air batteries, adapted from [16].

5.1. Aqueous Electrolyte

Aqueous electrolyte possesses highly ionic conductivity. Additionally, it is attractive for batteries with high power density. Additionally, water-based electrolytes are non-flammable and low-cost. However, the aqueous electrolyte is more corrosive than an organic solution. On the other hand, it has a limited water thermodynamic electrochemical window. The range of its thermal application is narrower, as its performance at low temperatures is limited by the freezing point [90]. Aqueous electrolytes can be grouped into three solutions based on the pH number [16].

Alkaline: The alkaline electrolyte solution has a pH value above 7 and lower or equal to 14, and is the most used electrolyte in the aqueous-based MABs compared to an acidic electrolyte, due to its favorable ORR with lower overpotential and faster reaction kinetics. However, when CO_2 from the air environment interacts with this electrolyte, it forms a carbonate surrounding the cathode. A high quantity of carbonate reduces the cathode's efficiency because it obstructs the pores of the positive electrode [16]. In addition, using strong alkaline electrolytes is harmful to the environment. Zinc-air and aluminum-air batteries usually use aqueous alkaline electrolytes. MABs with alkaline electrolytes can afford better electrocatalysis activity of oxygen and higher resistance to metal corrosion than neutral and acidic electrolytes. Examples of alkaline electrolytes include KOH, LiOH, and NaOH; however, the most employed in MABs is the concentrated KOH solution, due to it having the lowest viscosity and highest ionic conductivity [75].

The discharge behavior of the recently presented Si–air battery in the alkaline electrolyte has been investigated using different concentrations of KOH electrolyte. Silicon–air cell of refill type shown in Figure 8 was used. When the KOH concentration is between 2 M–5 M, the discharge potential dependence on the concentration is almost stable, while it decreases significantly only at lower concentrations up to 1 M, with the difference in discharge potential between high and low concentrations being 100 mV. In contrast, there was no impact of the KOH concentration on the open cell potential in this experiment. Because OH^- alters the conductivity and activity of the electrolyte, increasing the KOH concentration up to 6 M resulted in a linear rise in ionic conductivity. The application of discharge current, as well as the concentration of KOH, may have an impact on the roughness of the Si surface [80].
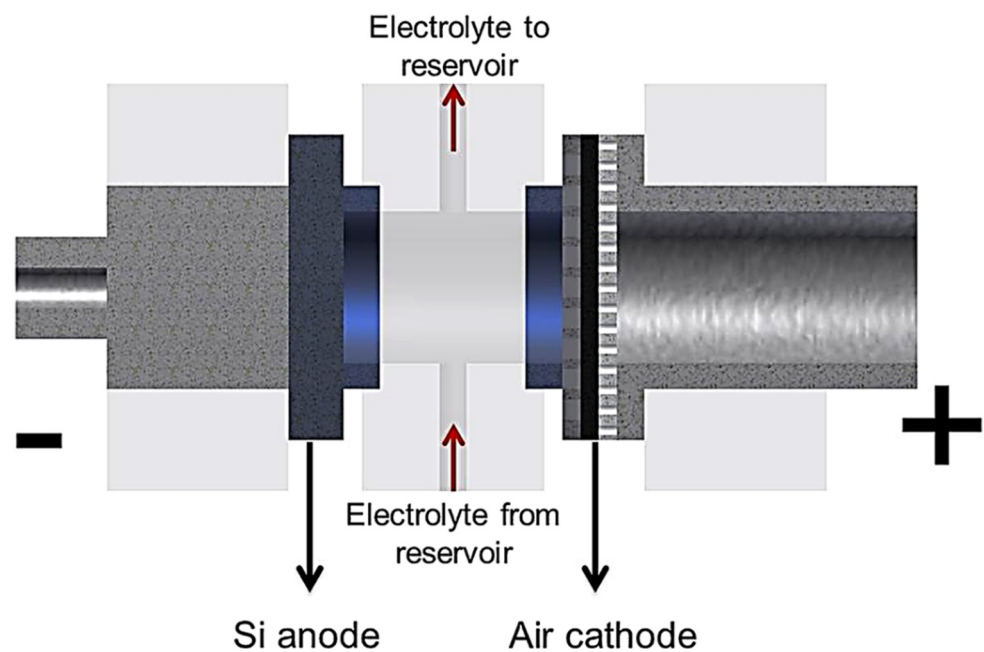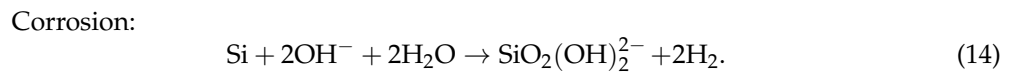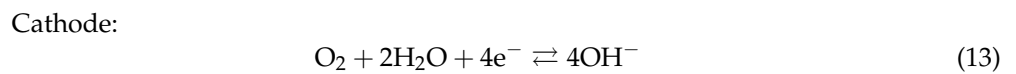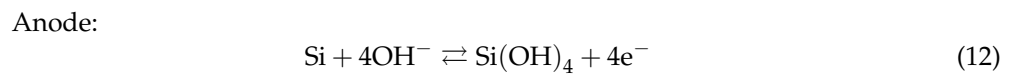

Figure 8. A refill type of Si–air cell, with permission to reproduce from [80].

Anode:

$$Si + 4OH^- \rightleftarrows Si(OH)_4 + 4e^- \qquad (12)$$

Cathode:

$$O_2 + 2H_2O + 4e^- \rightleftarrows 4OH^- \qquad (13)$$

Corrosion:

$$Si + 2OH^- + 2H_2O \rightarrow SiO_2(OH)_2^{2-} + 2H_2. \qquad (14)$$

Neutral: The neutral solution has a pH value of 7, and it has been demonstrated to increase both the cycle stability and the lifespan of secondary ZABs; however, at this time, no modeling studies have evaluated the performance of neutral ZABs in a laboratory setting. The pH stability of neutral ZABs is a key element in cell function. Additionally, an aluminum alloy–air battery can discharge with higher activity and lower corrosion rate in a neutral salt solution than in an alkaline electrolyte [16].

Acidic: The acidic solution has a pH between 2 and less than 7. It is rarely applied in aqueous-based MABs due to the decreased battery efficiency via a large amount of H + in the solution that reacts directly with metal. Different types of acids at the same pH, operation temperature, and concentration change an Al-Zn alloy anode's performance [16]. Acidic solution suppressed the formation of byproducts on the cathode and the formation of dendrite on the anode. However, it can result in corrosion problems for some types of MABs [91].

Electrolyte Additives

In an aqueous electrolyte, the metal electrode suffers from critical issues, including electrode corrosion, passivation, hydrogen evolution, and dendrite formation. The electrolyte material design can mitigate some of these issues by different electrolyte additives and enhance the metal electrode's performance. For alkaline conditions, the additives used can be ZnO and polyethylene or ZnO and carboxymethyl cellulose (CMC), as shown in Figure 9. Meanwhile, the additives for neutral salt water solution are Zn^{2+}, In^{3+} and Sn^{3+}. Additionally, some aromatic carboxylic acids are useful in alkaline solutions and have similar effects under acidic conditions. The imidazole group N atoms can be used in acidic solutions [75,91].
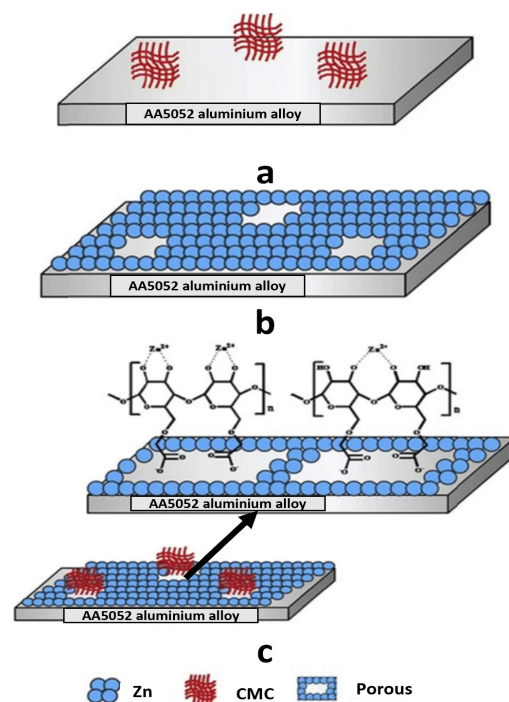

Figure 9. Corrosion protection for Al anode in NaOH containing (**a**) carboxymethyl cellulose (CMC), (**b**) ZnO, and (**c**) CMC/ZnO, adapted from [91].

5.2. Non-Aqueous Electrolyte

Solid-state electrolytes have the potential to minimize electrolyte leakage while maintaining thermal stability and robustness. They also have the potential to eliminate the problems of electrolyte evaporation and gas crossover. Another advantage is that it allows the increase in the energy density of MABs and the creation of reusable and bendable gadgets. Nevertheless, it has the potential to raise the battery's resistance and decrease its capacity. For MABs, the solid-based electrolyte has higher OH^- interfacial transporting resistance than aqueous system due to the poor wetting property that restricts the three-phase interface reaction, but using alkaline gel electrolyte (AGE) could mitigate these issues [16,75,91].

The ionic liquid electrolyte has two types of cations: (1) ions of alkali metal in an organic solvent and (2) large organic cations with inorganic/organic anions. This type of electrolyte has challenges due to carbonate formation that blocks the electrode pores and consumes the electrolyte [16]. Ionic liquids have low volatility, no flammability, and high ionic conductivity. Additionally, they can resist moisture in LABs. Ionic liquids that can be stored at room temperature (RTILs) are a kind of salt that has a melting point of less than 100 °C and is composed of large organic cations and organic/inorganic anions other things. Since MAB electrolytes may be very conductive, exceedingly nonvolatile, and can support the electrochemistry of certain metals, researchers have turned their attention to RTILs as MAB electrolytes as a result of the drying out problem [75,92]. RTILs are also expensive. The aprotic organic electrolyte is broadly used in MABs with metal electrodes that are unstable in water, such as Na and Li [75]. This contributes to the formation of a solid electrolyte interphase (SEI) at the surface of the anode. However, it has concerns for flammability, environmental, toxicity, and economic impacts. Additionally, an organic electrolyte results in a discharge product with nonconductive and insoluble properties that deposit and block the air cathode pores. A mixed electrolyte system has been proposed to solve the issues of cost, undecomposed discharge products, and poor efficiency of the round trip with organic electrolytes, all of which have been addressed [93].

5.3. Hybrid Electrolyte

A mixed electrolyte is also referred to as a hybrid electrolyte in certain circles. The name implies that it is composed of two distinct electrolytes separated by a solid electrolyte barrier that prevents water and gas diffusion while transferring cations. NASICON is one example of a solid electrolyte membrane, where it refers to sodium super ionic conductor [93]. The anode electrolyte in a hybrid battery system is called an anolyte, while the cathode electrolyte is called a catholyte. Using an alkali metallic ion (Na^+ or Li^+) solid-state electrolyte (SSE) separator, a novel aqueous iron–air battery was developed, including alkaline anolyte and acidic catholyte. When the anode and cathode are exposed to oxidation-reduction processes (redox reactions), the alkali metallic ion acts as a mediator of ionic transport [16,94]. Another example of a hybrid electrolyte battery system is the hybrid Na–air cell, which uses both organic and aqueous electrolytes, with a membrane separating them. Figure 10 shows the schematic diagrams for each cell compared to non-aqueous $Na\text{-}O_2$ batteries, with the comparative findings given in Table 8 [93].

Table 8. Comparison between non-aqueous $Na\text{-}O_2$ cell and hybrid Na–air cell [93].

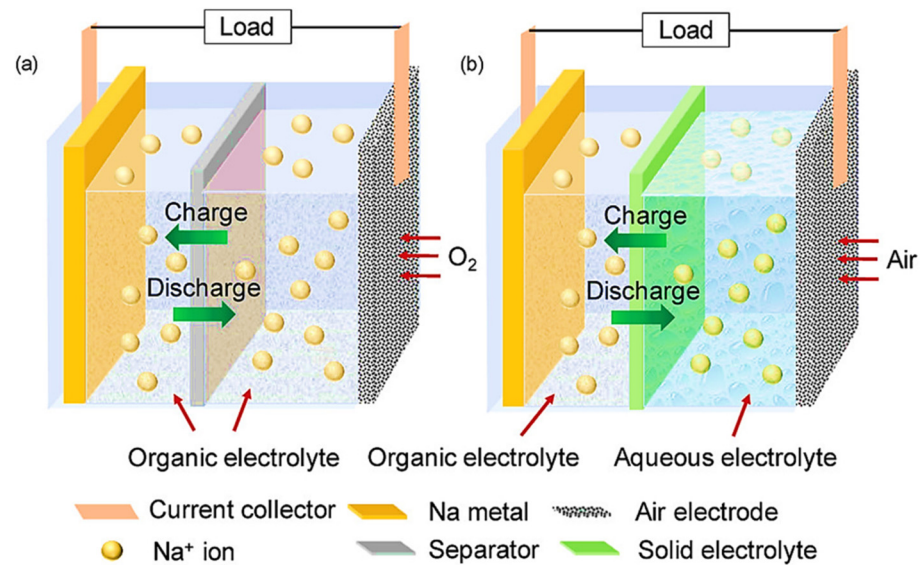|	$Na-O_2$	Na–Air
Barrier	Polymeric like Celgard 3501	NASICON
Discharge products	NaO_2 and/or Na_2O_2	NaOH
Product solubility	Insoluble	Soluble
Overpotential gap	Higher	Lower
Overall performance (%)	≥ 75	≤ 75
Stability	No recommendable	Recommendable
Safety	Satisfactory	Reasonable

Figure 10. A diagrammatic representation of (**a**) non-aqueous Na-O$_2$ battery (**b**) hybrid Na–air battery, adapted from [93].

Selecting the Electrolyte

In most cases, electrolytes are selected via a trial-and-error procedure based on rules of thumb connecting various characteristics of the electrolyte; as a result, time is spent in testing with different electrolytes to obtain the desired performance. In non-aqueous Li-O$_2$, Na-O$_2$, and K-O$_2$ cells, a connection was found between the solvent reorganization energy and the ORR rate constant k and the oxygen diffusion coefficient D (O$_2$), as shown in Figure 11. The research demonstrates the basic correlations that exist in the membrane between the solvent and the salt and the impact that these interactions have on the overall performance of the battery. With increasing cation size, it has been discovered that the rate of ORR in the presence of alkali metal ions is strongly dependent on the selection of salt anion as the size of the cation grows. For non-aqueous alkali metal–air batteries [95,96], the choosing of the electrolyte is made more accessible by using the graph shown below.
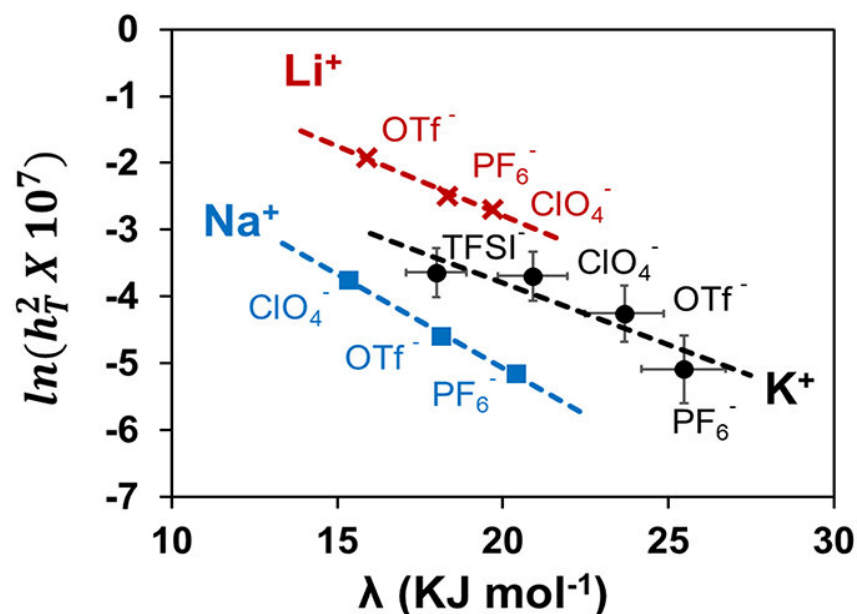

Figure 11. Correlation graph between solvent reorganization energy λ, the diffusion coefficient of oxygen D$_{O2}$, and the ORR rate constant k, adapted from [95,96].

Due to the fact that different kinds of MABs function differently, each type of electrolyte has benefits and drawbacks to consider. On the other hand, Table 9 highlights the benefits and drawbacks associated with each kind of MAB electrolyte.

Table 9. Comparison of different types of membranes for metal-air batteries.

Membrane	Types	Merits	Demerits	Reference
Aqueous	Alkaline	Potassium Hydroxide. Lithium Hydroxide. Sodium Hydroxide	Non-corrosive. Zn has rapid electrochemical kinetics as well as intrinsic electrochemical reversibility. Higher ionic conduction. ZAB has excellent performance at low temperatures. The solubility of zinc salts is very high.	CO_2 sensitivity is a concern. Alkaline solutions are harmful to the environment. Dissolution of Zn, precipitation of insoluble CO_3^{2-} hydrogen evolution, and electrolyte evaporation.	[16,75,97]
	Neutral	Potassium Chloride Lithium Chloride Zinc Dichloride Magnesium Dichloride	Secondary ZABs have excellent cycle stability as well as a long calendar life. Less corrosion and discharge due to high activity of Al alloy Carbonization of the electrolyte should be avoided. Dendrite formation may be reduced. Reduce the solubility of zinc in ZAB. CO_2 absorption is very low.	In industrial applications, this is a rare occurrence.	[16,58,97]
	Acidic	HCl HAc H_2SO_4 H_3PO_4 HNO_3	Reduced the development of byproducts on the cathode and the formation of dendrites on the anode.	Rarely utilized in industrial applications. Some kinds of MABs are prone to corrosion issues.	[16,91]
Non-aqueous	Ionic liquid	RTILs Lithium salts	Low volatility. Inflammability. High ionic conductivity. Excellent moisture resistance.	Carbonate crystallization. High purity is required. Synthesis is harmful to the environment.	[16,75,97]
	Organic	Sodium-based salts	Sodium and lithium-air batteries are among the most often used types of batteries. Contributes to the development of SEI at the anode.	Costly. Combustible. A certain degree of toxicity is present. The discharge product is preventing air cathode pores from opening.	[75,93]
	Solid-state	ZrO_2	Work in all MABs kinds without exception. Electrolyte leakage prevention, thermal stability, as well as robustness, are all important considerations. It is advantageous for increasing the energy density of MABs. Making wearable and flexible gadgets possible is made possible by this technology.	Increased resistance of the battery will result in a reduction in battery capacity. The wetting property is poor.	[16,75,91]
Hybrid	Alkaline anolyte and acidic catholyte.		Higher performance. Cycling stability is excellent.	In industrial applications, this is a rare occurrence.	[16,93,97]

6. Cathode of Metal-Air Batteries MABs

The cathode is the third part of MABs, and the active material for the cathode is oxygen from the surrounding environment, which is both free as well as plentiful. Furthermore, it does not require a hefty shell to keep it contained, which increases the device's energy density [97,98]. The oxygen reduction reaction (ORR) and the oxygen evolution reaction (OER) are the cathode reactions, with ORR occurring during the discharge cycle and OER occurring during the charge cycle [16,99].

6.1. Air Cathode Components

The air cathode is made up of a gas diffusion layer (GDL), a catalyst, and a current collector, as displayed in Figure 12. It can affect the properties of MABs greatly, so it must

be optimized by enhancing ORR, reducing the formation of carbonate and byproducts, avoiding flooding in the air cathode, and preventing evaporation of the electrolyte [91].
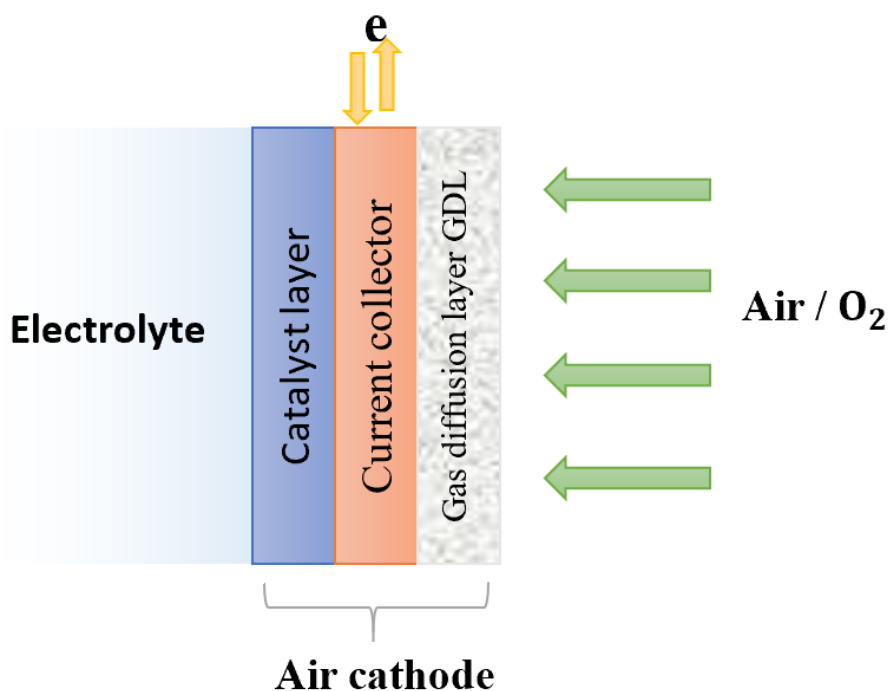

Figure 12. Air cathode components of MABs.

The current collector's primary tasks are connecting to external electrical circuits to create a closed circuit and transmit electrons between them. It may be made of non-metal or metal, with the metal current collector being made of porous foam-like metals such as Ni mesh, Cu, and stainless steel. Non-metal current collectors, such as carbon cloth, conductive carbon paper, and graphitic fiber, on the other hand, are made of carbon-based materials [16,91].

The gas diffusion layer (GDL) performs a variety of tasks. It acts as a conduit between the air atmosphere and the catalyst layer, allowing oxygen to diffuse into the atmosphere, or in other words, it absorbs air from the surrounding environment. Additionally, it inhibits electrolyte leaking out of the battery, stops water from entering into the battery, and it supports the catalyst layer of the battery. GDL should have the following characteristics: hydrophobicity, lightness, thinness, and high porosity. This necessitates meticulous planning ahead of time. Gas diffusion layers are often composed of carbon or catalytic materials and hydrophobic binders such as polytetrafluoroethylene PTFE (Teflon), while the catalytic materials are frequently combined with the binders before being put or imprinted onto current collectors [91].

The catalyst layer is the third component that has a significant effect on the characteristics of MABs. The bifunctional catalyst is required to increase the OER and ORR reactions, because the natural kinetics of the oxygen reactions is typically sluggish and increasing the kinetics of these reactions improves the electrochemical performance of MABs while simultaneously reducing overpotentials. The electrocatalysts may be divided into four categories, which are as follows: noble metals and their alloys, such as platinum Pt, iridium Ir oxides, and ruthenium Ru oxides, showing excellent performance in both OER and ORR tests; (2) metal oxides that are single, binary, or ternary in nature (e.g., MnO, NiO, and CoO); (3) carbonaceous materials, such as doped carbons and nanostructured carbons (e.g., nitrogen doping carbon); and (4) transition metals and metal macrocyclic complexes [28,37,49,50,91,99,100], respectively.

6.2. Oxygen Electrochemical Reactions in MABs

Since oxygen acts uniquely in aqueous as well as nonaqueous electrolytes (reaction pathways are shown in Table 10), it was necessary to develop a variety of catalysts that corresponded to distinct reaction processes. Both processes may occur on an air cathode electrode without the use of catalysts; however, since the natural kinetics of oxygen are sluggish, the use of electrocatalysts can speed up the reactions. The oxygen reduction reaction ORR and the oxygen evolution reaction OER are the two processes that occur when oxygen is present. This happens during the discharge process in MABs and consists of many stages, the most important of which are as follows: (1) oxygen diffuses into the surface of the catalyst from the surrounding environment. (2) Secondly, the surface of the catalyst absorbs oxygen. (3) The electrons from the anode are transferred to the oxygen molecules through an external circuit. (4) The oxygen connection is broken, and the oxygen bond becomes weaker. (5) The hydroxyl ion product is removed from the catalyst's surface and transferred to the electrolyte. All of these processes are reversible in OER, which happens during the charging process. Because of the relative stability of the intermediates generated following oxygen adsorption on the catalyst, either a four-step or a two-step route may be used in the ORR and OER processes, respectively. The superoxide intermediate produced by the two-electron mechanism is a reactive oxygen species.

$$O_2 + H_2O + 2e^- \rightarrow HO_2^- + OH^- \tag{15}$$

Table 10. Pathway reactions for the different electrolytes of metal-air batteries (MABs) [101,102].

Electrolyte		Oxygen Reaction	Reaction Pathway	
			Two-Step	Four-Step
Aqueous MABs	Alkaline	ORR	➢ $O_2 + H_2O(l) + 2e^- \rightarrow O^* + 2OH^-$ ➢ $O^* + 2OH^- + H_2O(l) + 2e^- \rightarrow 4OH^-$	➢ $O_2 + H_2O(l) + e^- \rightarrow OOH^* + OH^-$ ➢ $OOH^* + e^- \rightarrow O^* + OH^-$ ➢ $O^* + H_2O(l) + e^- \rightarrow OH^* + OH^-$ ➢ $OH^* + e^- \rightarrow * + OH^-$
		OER		➢ $OH^- + * \rightarrow OH^* + e^-$ ➢ $OH^* + OH^- \rightarrow O^* + H_2O(l) + e^-$ ➢ $O^* + OH^- \rightarrow OOH^* + e^-$ ➢ $OOH^* + OH^- \rightarrow * + O_2(g) + H_2O(l) + e^-$
	Acidic	ORR		➢ $O_2(g) + H^+ + e^- \rightarrow OOH^*$ ➢ $OOH^* + H^+ + e^- \rightarrow O^* + H_2O(l)$ ➢ $O^* + H^+ + e^- \rightarrow OH^*$ ➢ $OH^* + H^+ + e^- \rightarrow * + H_2O(l)$
		OER		➢ $H_2O(l) + * \rightarrow OH^* + H^+ + e^-$ ➢ $OH^* \rightarrow O^* + H^+ + e^-$ ➢ $O^* + H_2O(l) \rightarrow OOH^* + H^+ + e^-$ ➢ $OOH^* \rightarrow * + O_2(g) + H^+ + e^-$
Non-aqueous MABs	e.g., LAB in non-aqueous electrolyte	ORR	➢ $O_2 + e^- \rightarrow O_2^-$ ➢ $O_2^- + Li^+ \rightarrow LiO_2$ ➢ $2LiO_2 \rightarrow Li_2O_2 + O_2$	
		OER	➢ $Li_2O_2 \rightarrow 2Li^+ + O_2 + 2e^-$	

* is the active site on the surface, (*l*) is a liquid phase and (*g*) is a gas phase, O^*, OH^* and OOH^* are adsorbed intermediates.

The hydroxide OH^- produced in the four-electron process in an alkaline medium is presented in Equation (16).

$$O_2 + 2H_2O + 4e^- \rightarrow 4OH^- \tag{16}$$

The process of four electrons is highly required for high power and energy densities. Feeding purified air or employing an O_2-permeable membrane is necessary for alkaline media to avoid accumulating carbonate ions in the liquid electrolyte with time [100–102].

6.3. Progress Done in the Cathode of MAB

Although they have excellent performance, the electrocatalytic activity of noble metal-based electrocatalysts is limited by their poor durability and high cost [5,103,104]. In order to overcome these limitations, a study developed a graphene quantum dot/graphene hydrogel GH-GQD that has good durability and excellent electrocatalytic activity in alkaline solution in primary ZABs. Compared to GO and GH, the GQD exhibits a greater number of active sites, resulting in greater ORR electrocatalytic activity. Then, different concentrations of GQD (45 mg, 90 mg, and 180 mg GQD) were compared, and it was discovered that the GH-GQD-90 exhibited high ORR activity and excellent durability in alkaline primary MABs, high performance as an ORR catalyst in primary ZAB, and its discharge property performance at higher current densities can be compared with Pt/C. When used in MABs and fuel cells, the GH-GQD demonstrates tremendous promise for ORR as an alternative to noble materials [105].

An investigation into rechargeable MABs produced a one-dimensional manganese-cobalt oxide (spinel-type), $Mn Co_2O_4$ (MCO), and $CoMn_2O_4$ (CMO) nanofiber, as shown in Figure 13, that served as bi-functional cathode catalysts for the devices. As shown in Figure 14, these both have a high catalytic activity for both ORR and OER in an alkaline solution. Then, they were tested in ZABs as catalysts and were shown to decrease the gaps between the discharge and charge voltages significantly. As a result, the round-trip efficiency was improved as compared to a cathode without a catalyst. Despite repeated discharge–charge cycling, the CMO-NF, and MCO-NF catalysts maintain their stability; however, carbon corrosion in the catalyst/carbon composite cathode caused the battery's cycling performance to degrade significantly. A comparison of the electrochemical performance of ZABs utilizing the nanofiber catalysts that were manufactured with the performance of Pt/C and catalyst-free carbon cathodes is shown in Figure 15 [106]. It is possible that the structure of MCO-NF and OMC-NF, which facilitate mass movement via the porous one-dimensional structure and provide a high number of active reaction sites, is responsible for the enhancement of the electrochemical properties.
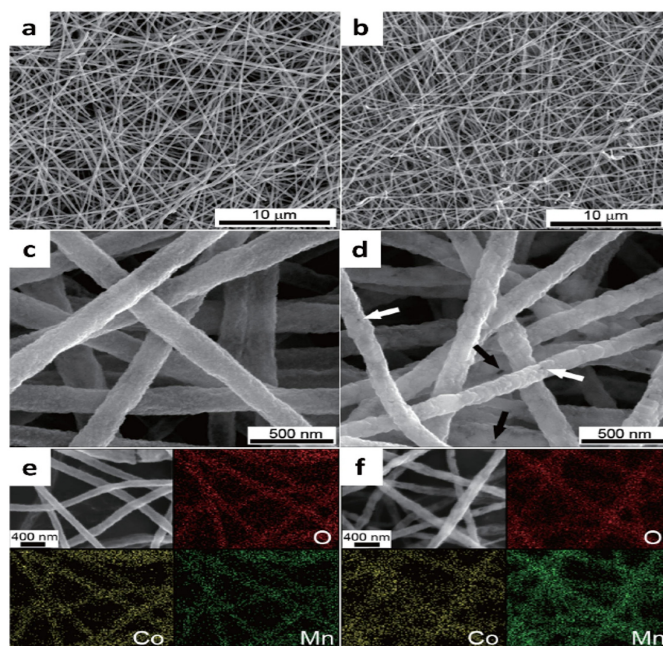

Figure 13. SEM micrograph of (**a–c**) MCO-NF and (**b–d**) CMO-NF. The arrows in (**d**) refer to pores on the fiber surfaces. EDS mapping data which present the element distributions of Co, Mn, and O for (**e**) MCO-NF and (**f**) CMO-NF, adapted from [106].
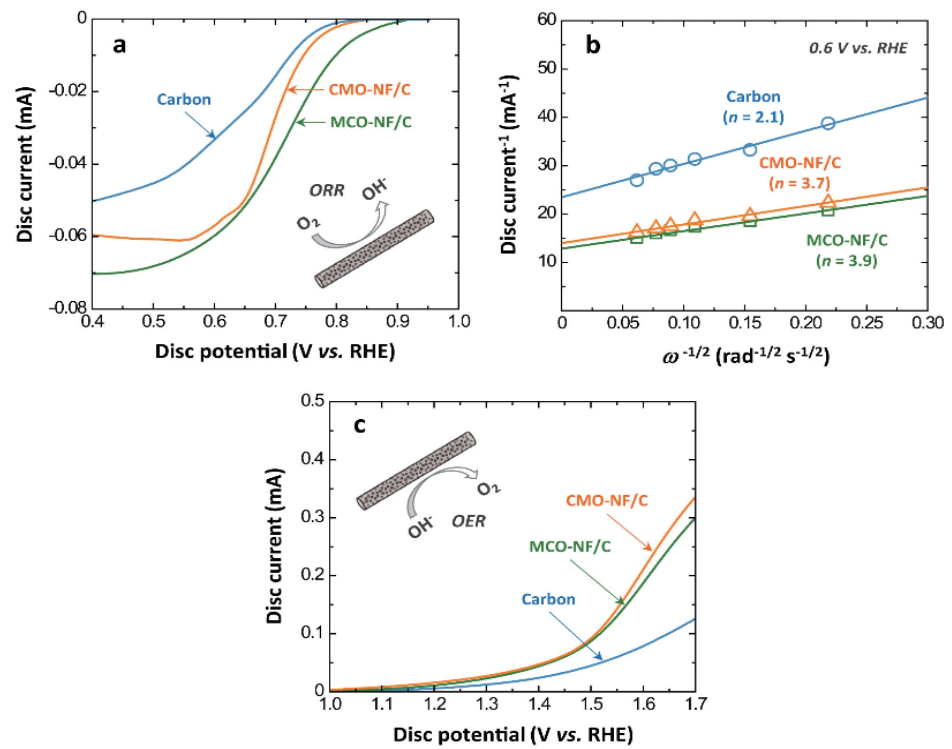
Figure 14. (**a**) Cathodic polarization curves at ω = 1200 rpm for the ORR measured, (**b**) K–L plots at 0.6 V vs. RHE and (**c**) anodic polarization for the OER, adapted from [106].
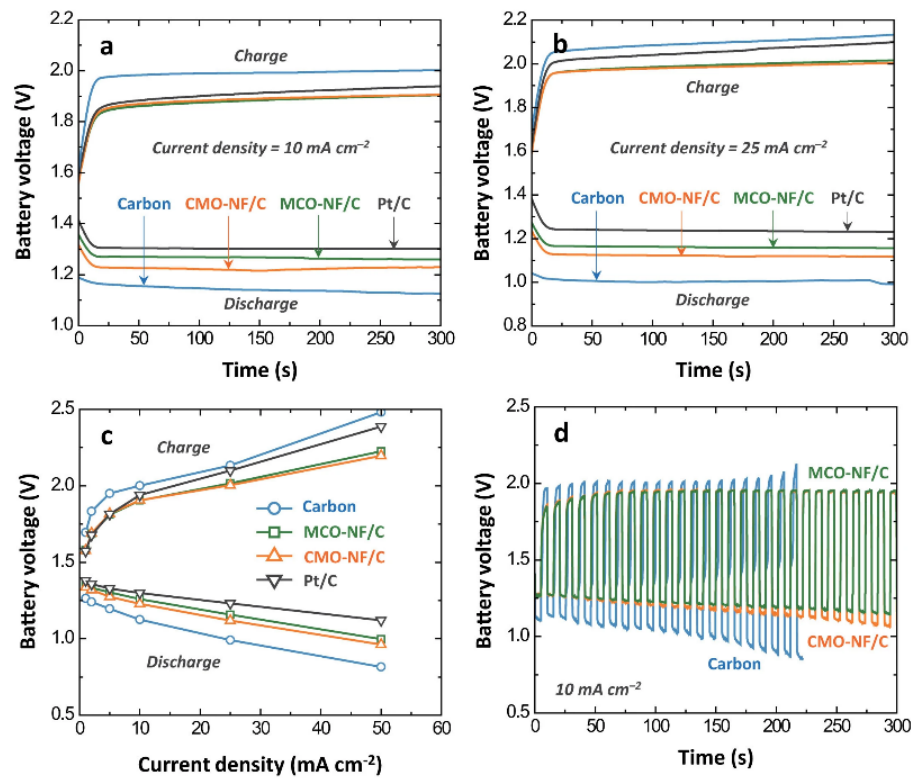

Figure 15. Galvanostatic discharge–charge plots (**a**) at 10 and (**b**) 25 mA cm^{-2}, (**c**) battery voltages at different current densities and (**d**) cycling performance at 10 mA cm^{-2} of rechargeable alkaline ZABs with various catalysts, adapted from [106].

To obtain Pt-based alternative electrocatalysts, a study mixed Ni, Co, and S to obtain a better electrochemical performance. Mixing sulfides and metal oxides containing transition

metals frequently showed useful electrochemical efficiency due to transition metal elements' synergy with single sulfide or metal oxide. $NiCo_2S_4$ hollow microspheres resemble a hydrangea and have a highly porous structure. The porous structure of $NiCo_2S_4$ may aid in the diffusion of oxygen and hydroxyl reactants, and it often has a high surface area for oxygen reactions due to its porous nature. When $NiCo_2S_4$ microspheres are tested in an alkaline medium, they exhibit good electrocatalytic activity for OER and ORR and high stability, making them a suitable catalyst for aqueous AABs and rechargeable ZABs. Moreover, the hydrangea-like structure exhibits numerously desorbed and adsorbed sites for oxygen. Therefore, $NiCo_2S_4$ microspheres can be evaluated for aqueous MABs as an advanced electrocatalyst [107].

In another study, a PdCo/C bimetallic nanocatalyst was prepared as a potential air cathode catalyst. The prepared catalysts went through a heat treatment process at 200 °C in H_2/Ar atmosphere from 4 to 24 h and the image for each period is presented in Figure 16. A clear correlation was found between the heat treatment and the total catalyst performance. The optimum heat treatment duration was 8 h, resulting in the greatest activity for ORR and OER. As a consequence, the HT-8 h PdCo/C catalyst was tested in rechargeable Zn–air and Mg–air batteries. The resulting performance of each battery is shown in Figures 17 and 18, respectively, to demonstrate its effectiveness. When the HT-8 h PdCo/C catalyst is used, the stability and activity of the Zn–air and Mg–air batteries are improved, and the activity is increased, indicating that it has the potential to be used on a broad scale [108].
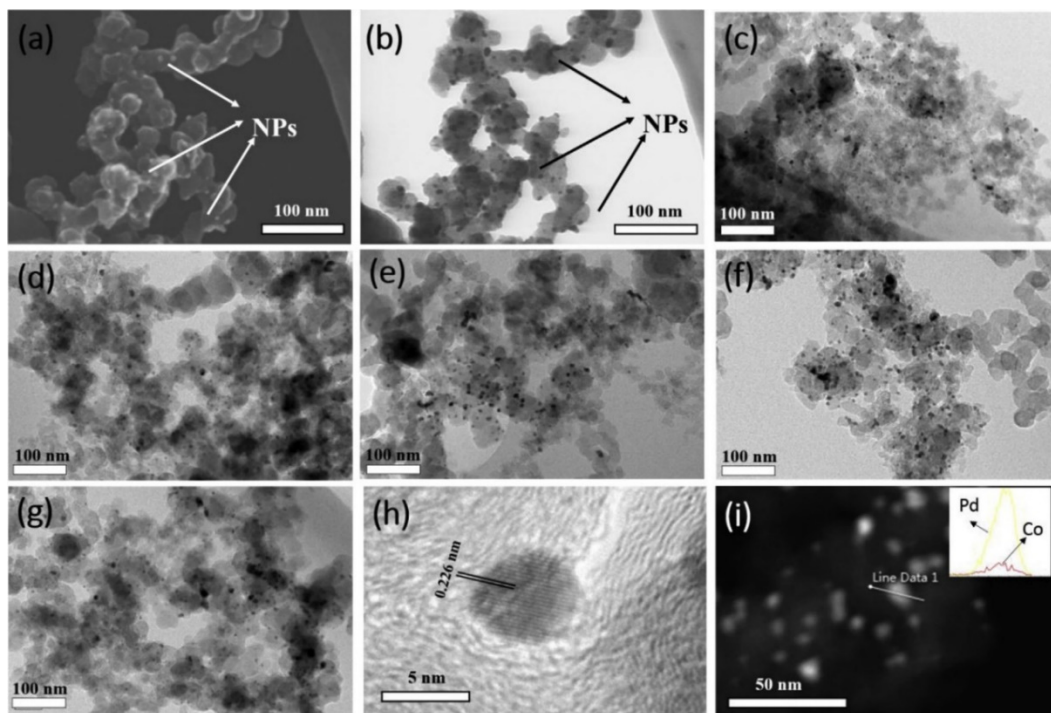

Figure 16. The HT-0 h PdCo/C catalyst (**a**) SEM and (**b**) STEM images. TEM images of (**c**) HT-0 h, (**d**) HT-4 h, (**e**) HT-8 h, (**f**) HT-16 h and (**g**) HT-24 h PdCo/C catalysts. The HT-8 h sample (**h**) HRTEM image and (**i**) EDS line scanning profile, with permission to reproduce from [108], License number: 5152750650685.
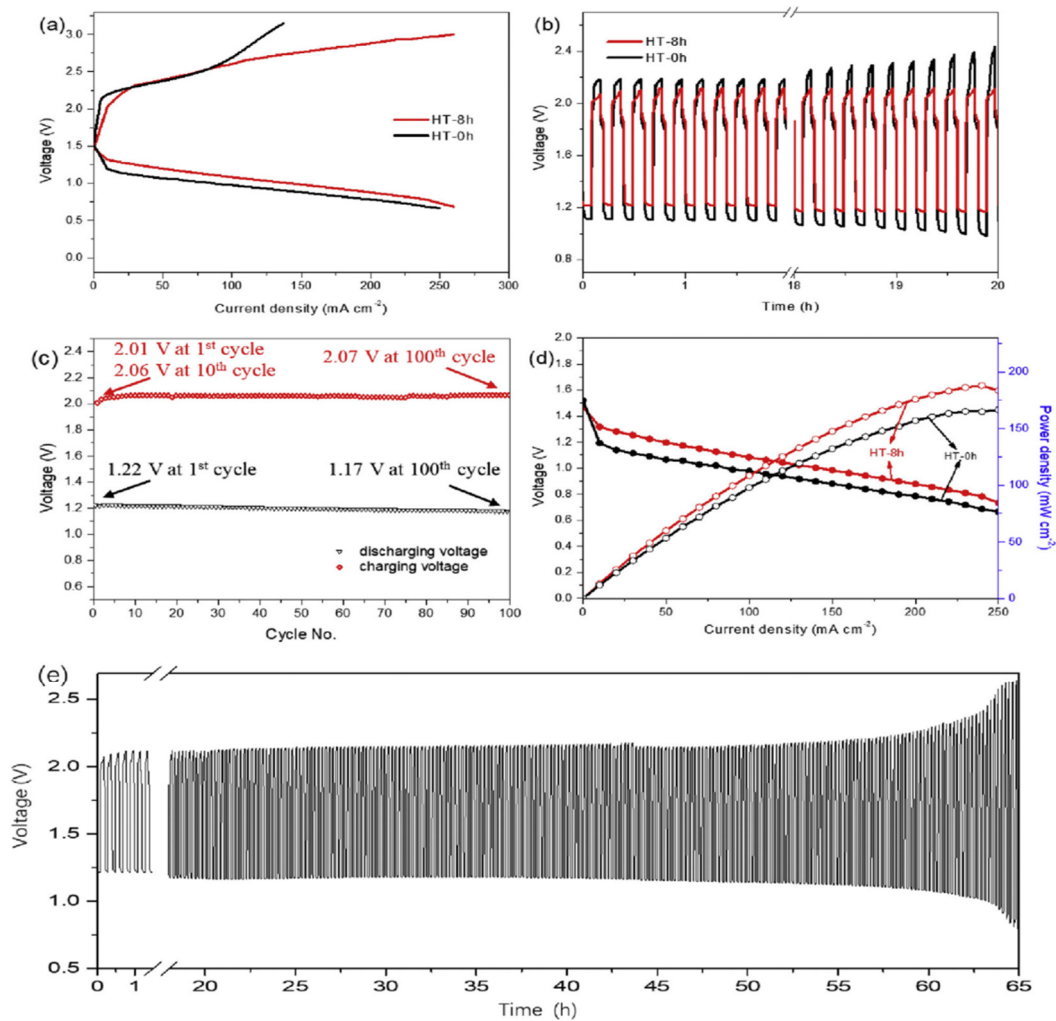
Figure 17. ZAB's performance with PdCo/C catalysts. (**a**) Polarization curves, (**b**) discharge and charge voltage profiles for the first 20 h, (**c**) discharge and charge state end voltages for the consecutive 100 cycles of the HT-8 h sample through the first 20 h, (**d**) discharge polarization, and power densities curves and (**e**) battery long-term cycling stability using the HT-8 h catalyst, with permission to reproduce from [108], License number: 5152750650685.
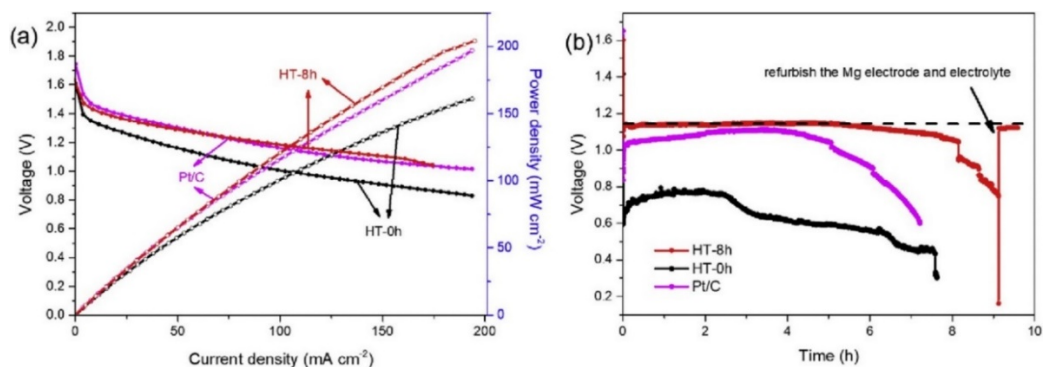

Figure 18. (**a**) Discharge polarization and power densities curves and (**b**) discharge stability curves of the HT-8 h, HT-0 h, and Pt/C in MABs, with permission to reproduce from [108].

A novel technique for manufacturing air cathodes is described in Figure 19, which employs cost-effective ways to reduce the cathode structure while maintaining high quality. The effect of temperature on the manufactured in-house air cathode can be seen in the polarization curves shown in Figure 20A and Table 11, respectively. The research team

utilized various characterization methods to further understand the performance and characteristics of the newly created air cathode, which was then compared to commercial air cathodes for comparison. Since the developed air cathode does not require the heat seal coating materials that are used in the commercial air cathode, the gas flow restriction and internal electrical resistance of the system are both reduced, allowing for an increase in water transportation to reaction sites as well as an increase in air permeability. As demonstrated in Figure 21, the performance of the magnesium–air single cell utilizing manufactured air cathodes is comparable to that of a commercial air cathode [109]. The newly designed air cathode, on the other hand, is both cost-effective in terms of production and materials and appropriate as a cathode for an MAB in a neutral or alkaline electrolyte.
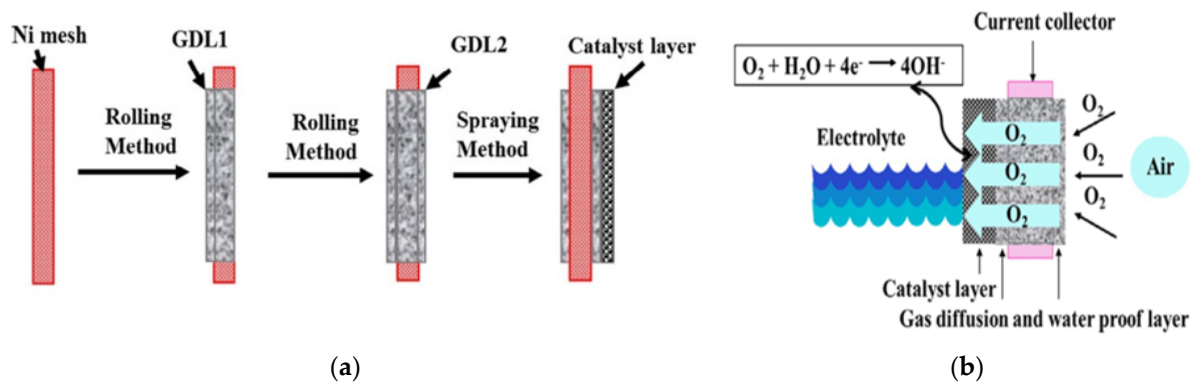

(**a**)　　　　　　　　　　　　　　　　　　(**b**)

Figure 19. Schematic of (**a**) the fabrication process of the air cathode and (**b**) diagram of the fabricated air cathode, adapted from [109].
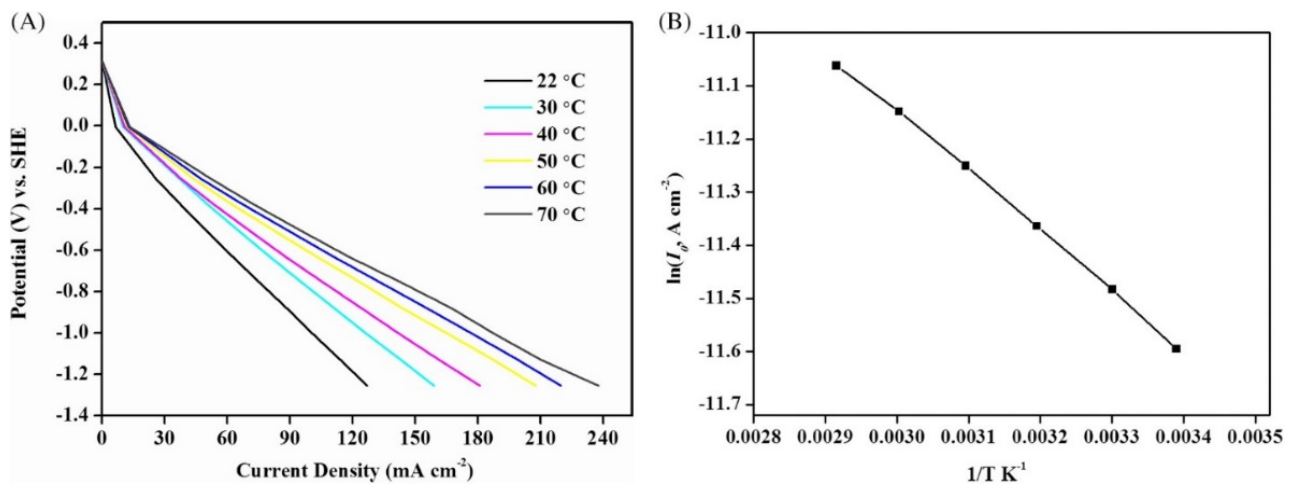

Figure 20. (**A**) LSV curves of developed air cathode in NaCl solution at different temperatures and (**B**) ln I_o of the cathodic ORR plot as a function of the temperature reciprocal (data from Table 11), adapted from [109].

Table 11. The ORR performance of advanced air cathode in air-saturated 10 wt% NaCl solution at a different temperature was adapted from [109].

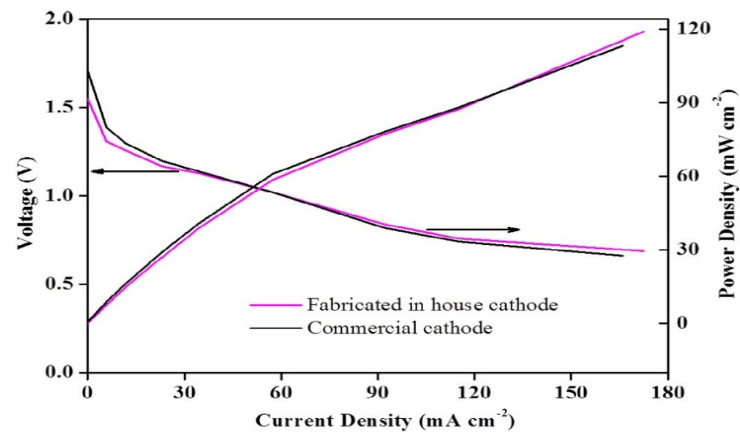| Temperature (°C)	Current Density (mA cm^{-2}) at -1.55 V (vs. SHE)	Geometric Exchange Current Density (mA cm^{-2}) at Ambient Pressure
22	127	9.21×10^{-3}
30	158	1.03×10^{-2}
40	182	1.16×10^{-2}
50	205	1.30×10^{-2}
60	224	1.44×10^{-2}
70	238	1.55×10^{-2}

Figure 21. Mg–air single cell performance with the commercial cathode and fabricated in-house air cathode in neutral solution adapted from [109].

The non-aqueous LAB was used to investigate the effect of the operating temperature on the morphology of the discharge product produced. The solid discharge product Li_2O_2 clogs the cathode pores, thus stopping the discharge process. The product must be oxidized before it can be used in the charging process. Following the application of various operating temperatures at varying discharge current densities, the morphology of the Li_2O_2 discharge product and the performance are shown in Figures 22 and 23, respectively, after the application of different operating temperatures.
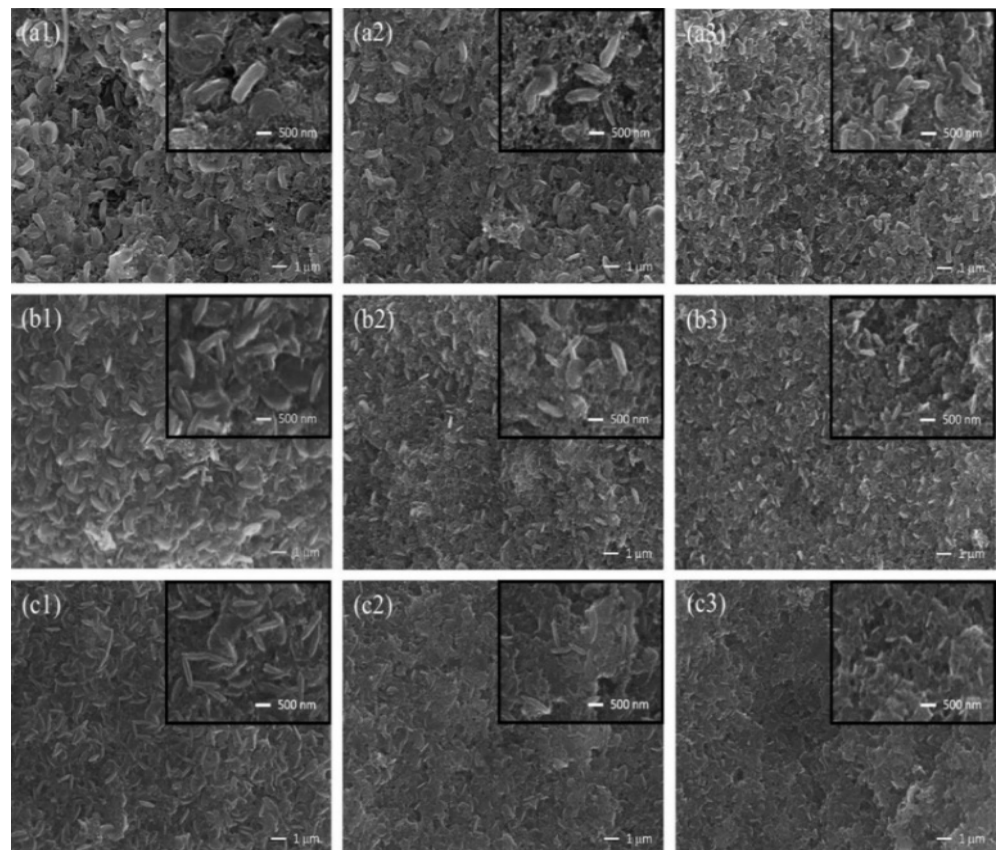

Figure 22. Cathode SEM images after discharge (5000×) at (**a**) 0.1, (**b**) 0.2, and (**c**) 0.3 mA cm^{-2} discharge current densities and at temperature sof (**1**) 21, (**2**) 35 and (**3**) 45 °C, with permission to reproduce from [110].
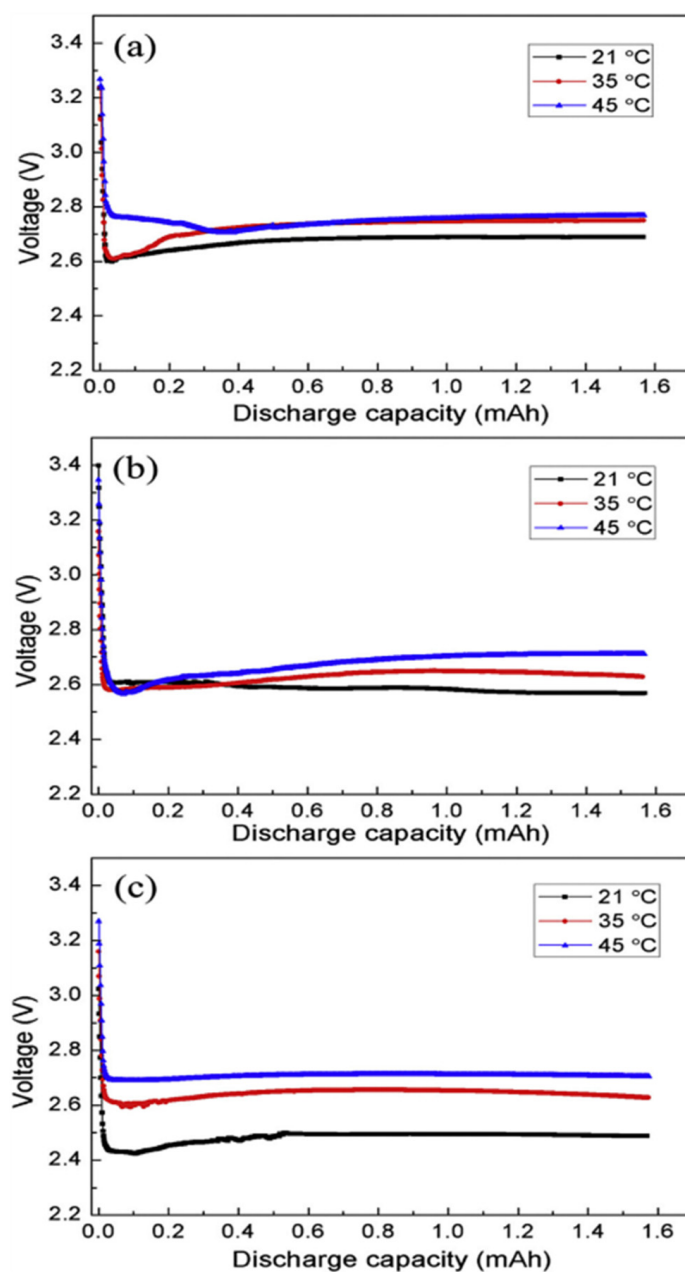
Figure 23. Discharge curves at different temperature and at current density (**a**) 0.1, (**b**) 0.2, and (**c**) 0.3 mA cm^{-2}, with permission to reproduce from [110].

This is in addition to Figure 24, which depicts the voltage–capacitance graphs at various temperatures. It is concluded that altering the operating temperature at a certain discharge current density does not affect the form of Li$_2$O$_2$, while raising the operating temperature causes a reduction in the size of the discharge product. Additionally, the form of the discharge product at a given temperature change in relation to the discharge current density. Finally, the operating temperature impacts the charge voltage, cyclability, and capacity of a particular non-aqueous LAB [110].
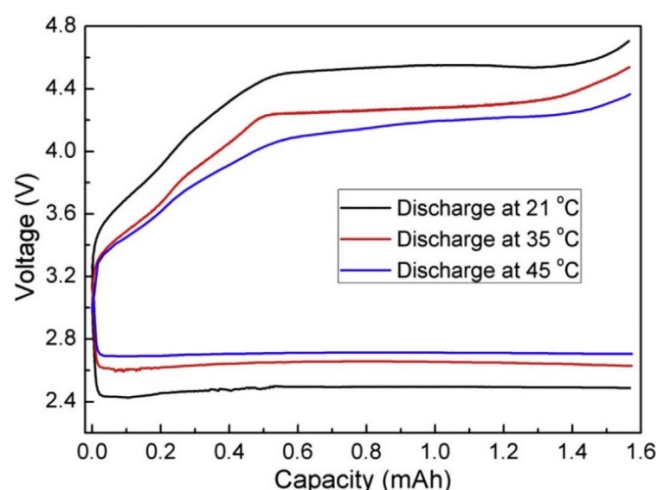
Figure 24. Charge curves at the battery operating temperature of 21 °C with discharge at different temperatures, used with permission to reproduce from [110].

7. Progress in the Design of the MABs

The two kinds of MABs are primary and secondary, as highlighted in Figure 25a–c. Primary MABs are non-rechargeable, while secondary MABs are rechargeable. The main MABs have two electrodes, each with an ORR catalyst, while the rechargeable MABs have two or three electrodes, each with an ORR and OER catalyst, depending on the model. In the three-electrode arrangement, the metal electrode is located between the air cathode electrode and the charging electrode for the OER, which is a convenient position. The air cathode is electrically separated during the charging process, which extends its lifespan by preventing it from being exposed to the high oxygen evolution reaction potential during the charging phase. In contrast, the two-electrode design of rechargeable MABs, shown in Figure 25c, consists of a metal electrode and a bifunctional air electrode that contains catalysts for ORR and OER, as well as other functions. This arrangement is straightforward and does not need the separation of the two electrolyte flows, since the air cathode may serve as both an anode for OER and a cathode for ORR [99]. Furthermore, it has less mass (resulting in higher specific energy) and fewer interfaces, which reduces the possibility of kinetic rate losses. Additionally, recent research has focused on improving the stability and efficiency of bifunctional catalysts [111].
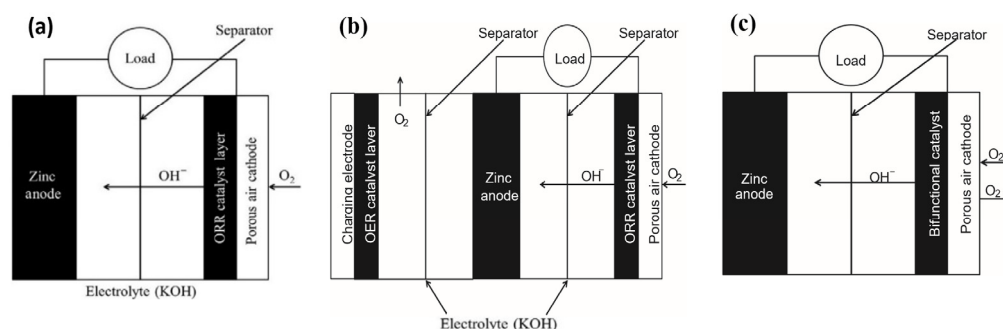

Figure 25. (**a**) Primary Zn–air cell; secondary Zn–air cell in (**b**) three-electrode design and (**c**) two-electrode design with a bifunctional catalyst layer, adapted from [111].

7.1. Classifications Cell Structure

Figure 26 illustrates the classification of MABs into three configurations: the conventional static battery, the flow battery, and the flexible battery. The first configuration is the traditional static air battery, which consists of the three primary components (anode, cathode, and electrolyte) and a separator. In this configuration, the kinetics of the anode

reaction are fast compared with the cathode reaction, and it requires highly efficient catalysts to facilitate the reactions, in addition to the challenge of the by-products that deposit insolubly on the surface of the electrodes during charge-discharge cycles, resulting in a decrease in the battery's performance due to the blocking of the pores of the electrode, limiting the air diffusion step. The second configuration is the flow battery, which consists of an anode, cathode, electrolyte, separator, and electrolyte bank, and to drive the electrolyte flow, it is usually installed with a pump. The configuration of the electrolyte flow decreased the volume density and energy efficiency; also, additional tubes and pumps increased complications during the discharge process. The third configuration is the flexible battery, which is of huge interest due to the increasing demand for flexible, portable electronics in recent years which require a flexible energy storage device. This type of battery consists of a thin metallic plate anode to reduce battery weight, a cathode such as carbon fiber, a highly conductive electrolyte, and a separator. Currently, the ideal flexible batteries are ZABs and aluminum-air batteries, due to their safe operation, high energy density, and low cost [16].
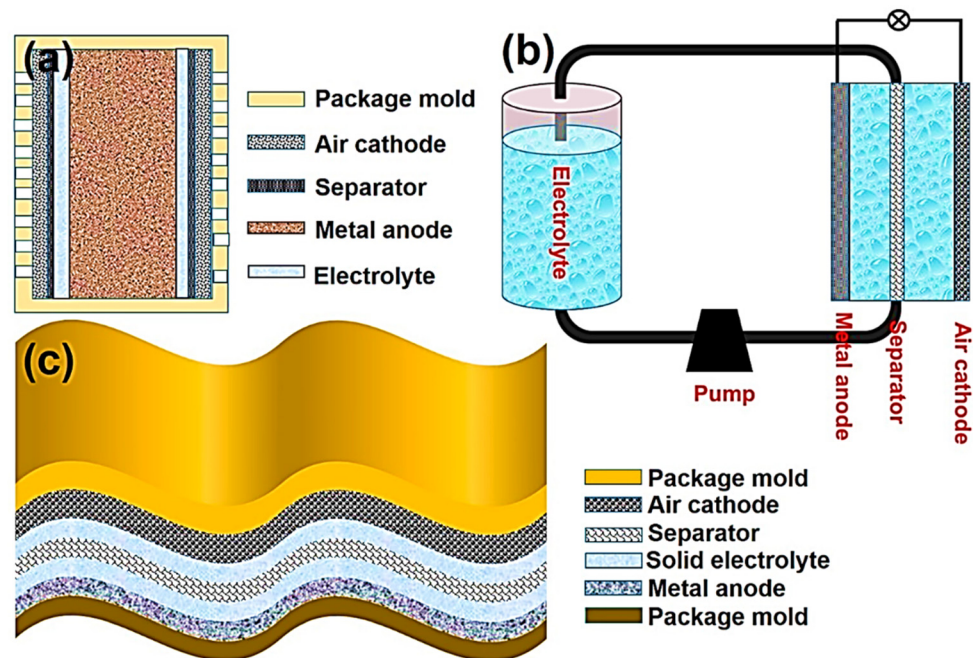

Figure 26. Configurations of MABs in a (**a**) multi-cell static battery, (**b**) flow battery and (**c**) flexible battery, adapted from [16].

7.1.1. Static MABs

In addition to tiny and portable electronic gadgets, the static system may also be used for large-scale electronics. Metal–air batteries with a static structure have been extensively researched; however, their performance is restricted regarding practical power/energy density and energy efficiency, respectively. The integration of static cell structure with other energy technologies, on the other hand, is complicated and difficult [112].

Parallel-Plate Electrode Configuration

The arrangement of the parallel-plate electrode configuration shown in Figure 27 allows high heat dissipation and mass transport rates. For laboratories, small cells are favored due to the low requirements of power and volume. However, the heat generated in large cells during the charge and discharge cycles has to be considered. The cross-section of a unit cell and the stack connecting several cells together to form a battery are displayed in Figure 28 [51]. Several materials are investigated in air cathodes such as Pt/C combined

with Ir/C, and urchin-like NiO_2S_4 microspheres covered by a sulfur-doped graphene nanosheet, S-GNS (S-GNS/NiO_2S_4) [113].
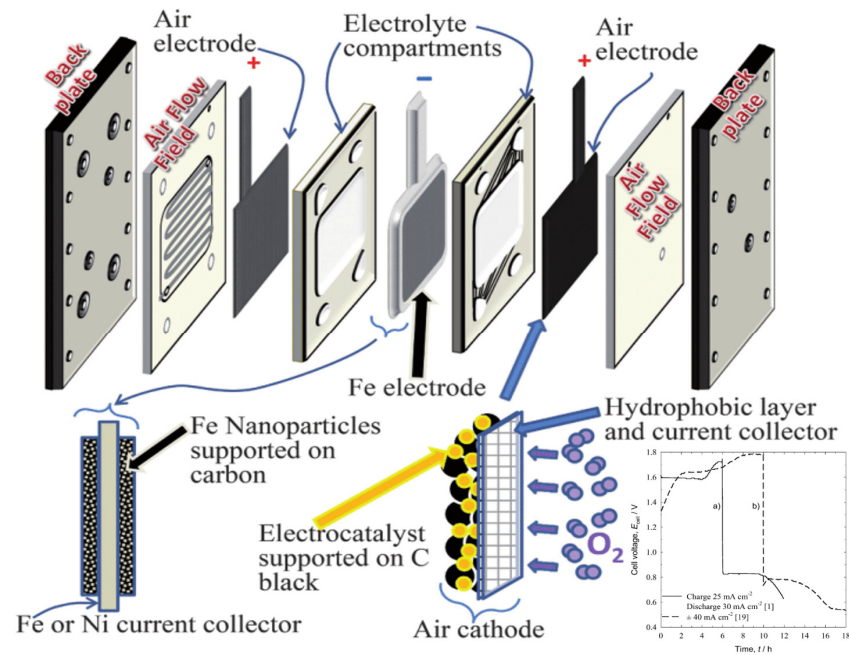

Figure 27. Parallel-plate electrode configuration of Fe–air battery, adapted from [51].
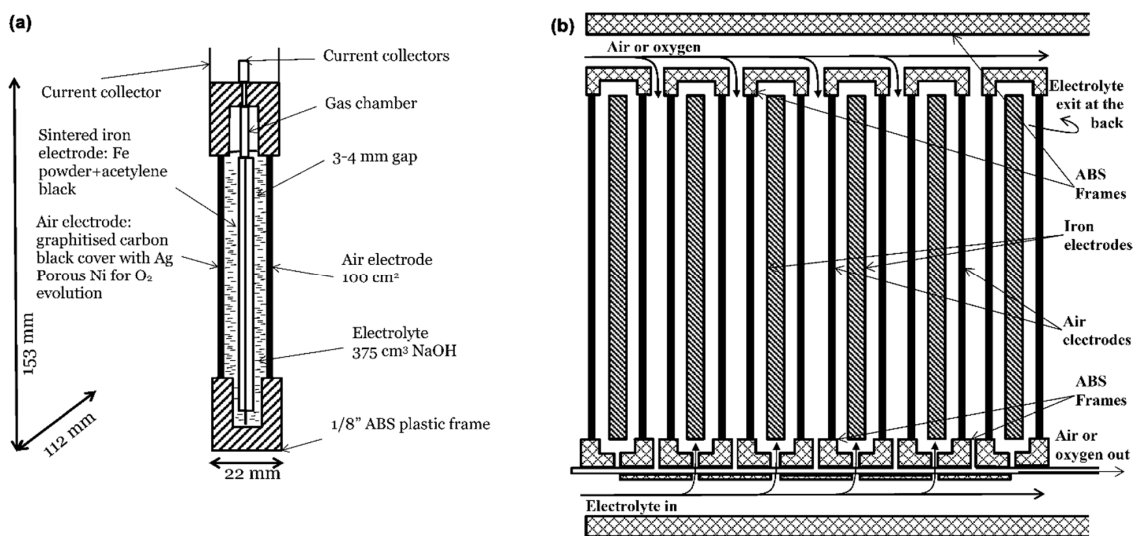

Figure 28. Fe–air unit cell. (**a**) Single-cell cross-section and (**b**) stack of 6 Fe–air cells, adapted from [51].

Coin-Type

A coin cell type and its components are shown in Figure 29, and Figure 30 displays the performance of this configuration using different electrolytes at 6 M concentration: potassium hydroxide (KOH), poly vinyl alcohol (PVA), poly acrylic acid (PAA), and PAM [114].

In Situ Cell

Numbered components of an in situ cell are shown in Figure 31. The alloy clamp rings and PEEK screws, used to close the cell after assembly, are numbered 1 and 2, respectively. The thin sheets of Ni metal (used as negative and positive electrodes) are numbered 3 and 4, respectively. The tubing connections for pumping the electrolyte or gas fuel are numbered 5. The thyristor is numbered 6.
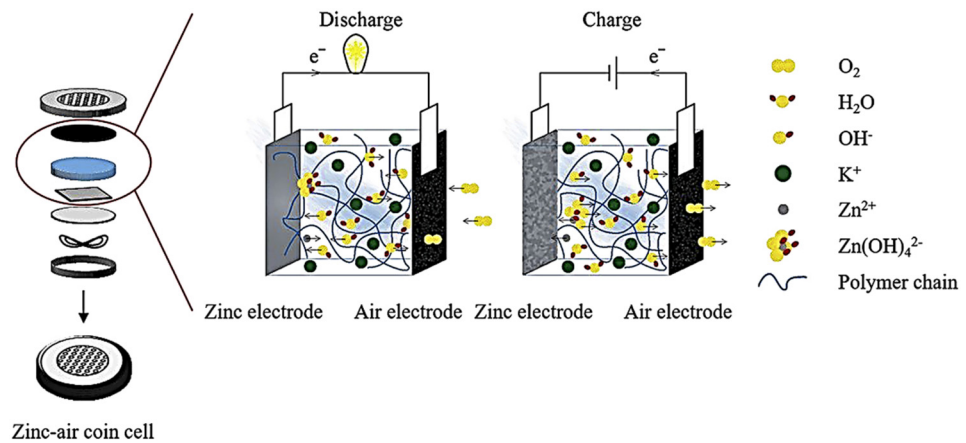
Figure 29. Schematic diagram of a coin cell, with permission to reproduce from [114].
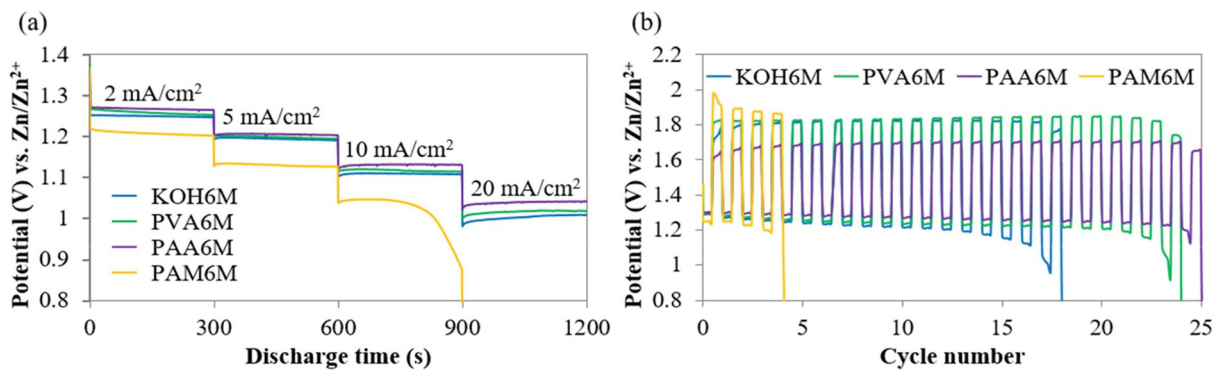

Figure 30. Zn–air coin cell: (**a**) discharge curves at different current densities and (**b**) discharge–charge cycling performance at 0.5 mA cm^{-2} using various electrolytes, with permission to reproduce from [114].

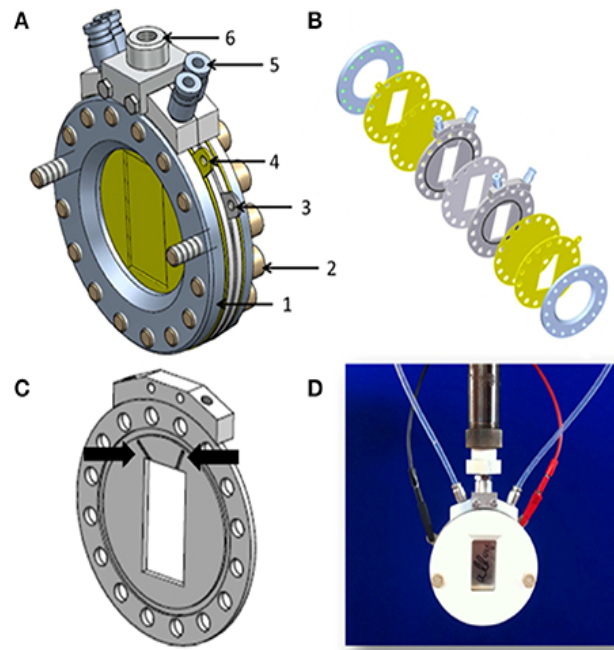**Figure 31.** (**A**) Schematic diagram of in situ cell. (**B**) The cell components sketch. (**C**) Close-up view of the separator module (the black arrows represented the apertures which connect the battery inner compartment with the cell exterior). (**D**) Real assembled cell, adapted from [115].

7.1.2. Flexible MABs

The stability of the flexible MABs should be ensured when subjected to frequent mechanical strain over an extended time period, and the security of the battery should be ensured when subjected to a variety of deformation circumstances. The electrodes in flexible MABs must have the ability to adapt to changing conditions. Metal ribbons, metal rods, metal foil, or a flexible metal substrate covered with a metallic powder may be used as anodes, as can metal rods coated with a metallic powder. Additional characteristics of a cathode current collector include great flexibility, high conductivity, and air permeability. These characteristics should be combined with an active material coating to produce a flexible air cathode. The carbon materials with the greatest potential as active materials are graphene and nanotubes, which are distinguished by their high tensile strength and high Young's modulus. As a bonus, putting metallic or metal oxide/nitride on a carbon substrate enhances the cathode's catalytic activity [16]. The remarkable performance of the flexible MABs is attributed to the close contact that exists between the cell components [116].

Fiber-Type

The configuration of this type of flexible MAB and the progress made in its development are shown in Figure 32. The cell structure of this type of MAB is usually a polymer electrolyte (e.g., gelatin gel polymer electrolyte GGPE) around the central metal anode and flexible air cathode coated with the electrolyte. It can operate efficiently under external strain. Additionally, other studies demonstrated the excellent mechanical stability and electrochemical performance of this configuration type [116].
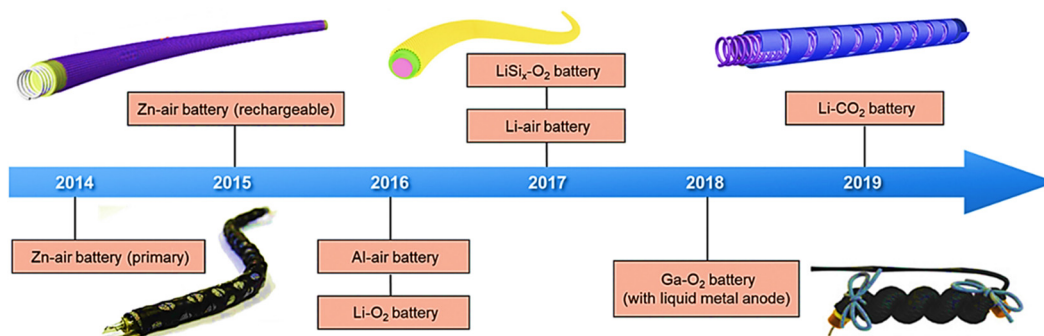

Figure 32. Schematic showing the progress made in the development of fiber-shaped metal-air batteries [117].

Sandwich-Type

The components in sandwich-type MAN are produced in plan form, then assembled as in Figure 33. This configuration exhibited high volumetric and gravimetric energy density and excellent electrochemical and cycling performance under bending conditions even at a high current density [116,118].

Array

A planner multilayer MAB array configuration is presented in Figure 34. It possesses flexible and stretchable properties, a thickness of nearly 3 mm, and exhibits excellent stable and rechargeable battery performance. This array can be connected in series and parallel, or in a combination between them. It can be used in wearable devices [69].
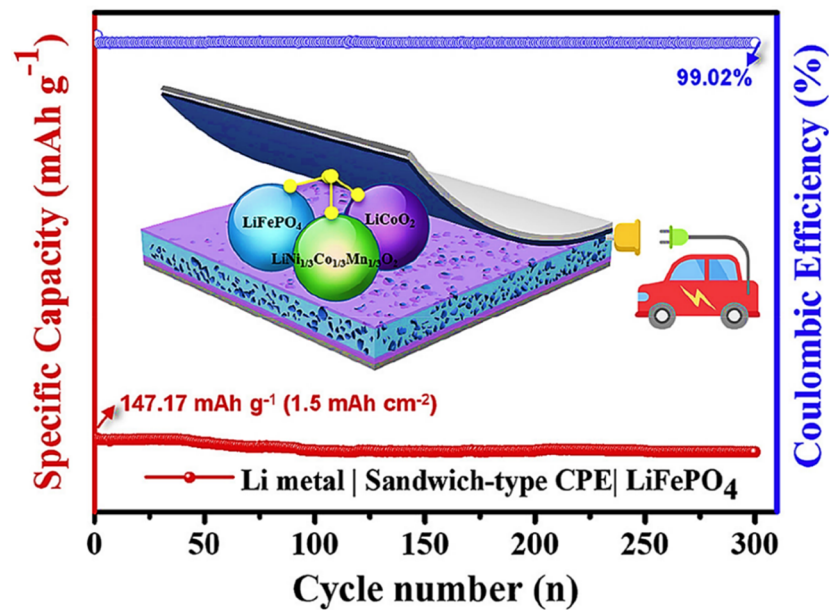
Figure 33. Stability of sandwich-type Li metal battery (inset shows schematic of the cell) [118].

Figure 34. (**a**) Multilayered structure of a flexible/stretchable rechargeable ZAB array and (**b**) bending and stretching the battery and different array connections series and parallel, with permission to reproduce from [119].

7.1.3. Flow MABs (MAFBs)

The flow system is adaptable and can be readily combined with different energy technologies when it comes to cell construction. It is safe and has a long operational life because of the flow of the anolyte/electrolyte, minimizing side reactions. It has the potential to be used for large-scale energy storage as well as stationary power plants. The anolyte circulation is, however, depicted in Figure 35 [120].

Figure 35. Schematic diagram of MAFBs' anolyte circulation [120].

Anolyte Circulation

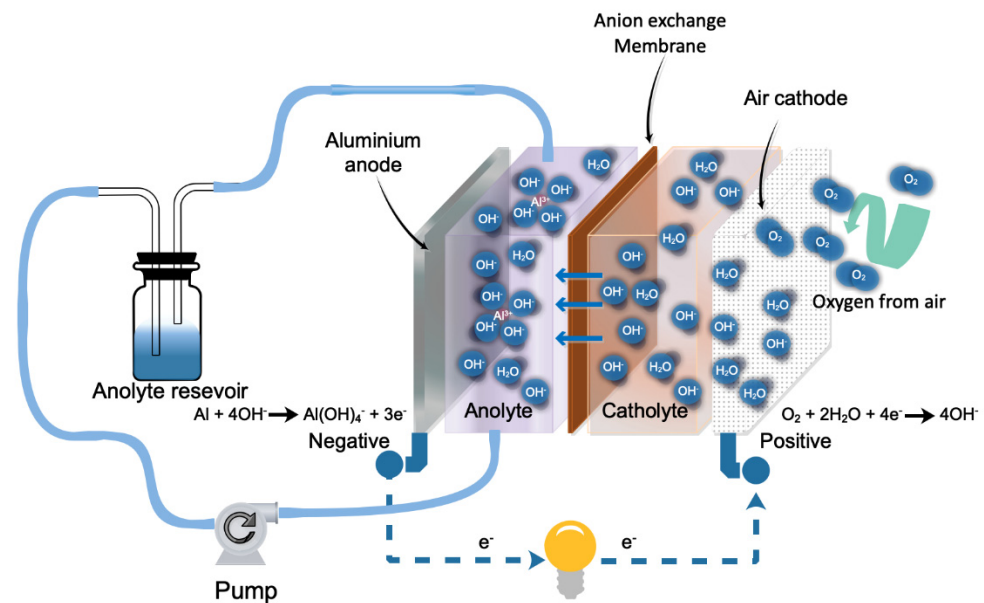The system consists of an anode electrode, an ion transport membrane, catalysts, a casting air electrode, and two current collectors. The cell in Figure 35 uses a flow of a redox couple at the negative electrode, while it uses air or oxygen at the positive electrode. The flow rate of the anolyte must be controlled to avoid any possible concentration polarization. Replacing the positive electrolyte tank that used conventional redox flow batteries REBs with an oxygen GDE reduces the volume and total weight, thus improving the power and energy densities. Vanadium–air and zinc-air flow batteries (VAFB, ZAFB) are an example of this approach towards metal–air flow batteries [112,120].

Electrolyte Cycling

This approach is presented in Figure 36A, where the fresh electrolyte continuously supplies the flow through the electrochemical cell. It increases the metal anode charge and discharges efficiency, and at the same time, it eliminates the by-products and the side reactions. Therefore, the cathode becomes less blocked, which is favorable for oxygen access. Sodium-air, zinc-air as well as lithium-air flow batteries can be fabricated using this approach, and Figure 36B shows the efficiency of zinc-air flow batteries using a NiS_x-FeO_y/sulfur-doped carbon fiber paper SCFP catalyst [112].
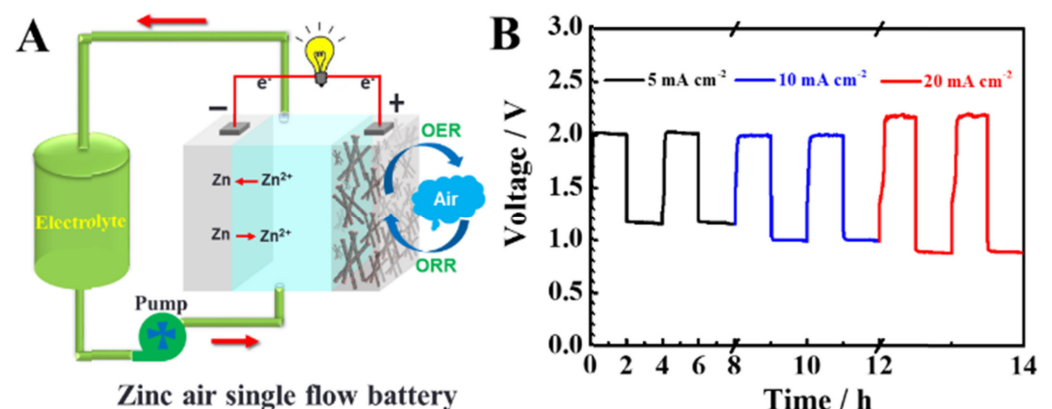

Figure 36. (**A**) The schematic diagram and (**B**) the charge-discharge curves of the assembled ZAFB, adapted from [121].

Hybrid Electrolyte Flow Battery

Since some metals, such as Na and Li, are water-sensitive, and thus their use is questionable in aqueous media. Inorganic/organic hybrid electrolytes separated by a plate that is a superionic conductor are suggested in their flow configurations. Additionally, this concept has been widely improved in static sodium and lithium–air batteries to protect the aprotic electrolyte and protect the highly reactive the Na/Li metal anode from oxygen crossover or water and carbon dioxide impurities in ambient air [112].

Bidirectional Flow Battery with a Two-Layered Cathode

The bidirectional flow battery components of vanadium–air flow battery (VAFB) are shown in Figure 37, where it used an exchangeable gas diffusion electrode with a different catalyst for both charging and discharging processes. Involving this developed cathode in VAFB resulted in 44.5% voltaic efficiency and 87.6% coulombic at 40 mA cm^{-2} (used catalyst Pt/C and IrO$_2$), but highly active electrocatalysts and crossover-minimizing membranes need to be collectively improved [112]. For example, in a vanadium redox flow battery, the crossover of vanadium species through the ion-exchange membrane (IEM) is a serious problem that leads to continuous capacity decay. To decrease this problem, tungsten oxide nanofiller with different mass loadings (0–20 wt.%) was introduced in the Nafion matrix [122]. The lowest vanadium species crossover was achieved using 20% wt. of WO$_3$. The coulombic efficiency, energy efficiency, and capacity retention were enhanced by 93%, 75% and 62%, respectively, as compared to 88%, 65%, and 42%, respectively, in the case of using pristine Nafion 212. Additionally, the electrode materials and their cost have a great effect on the development and commercialization of flow batteries. For instance, in addition to the selection of mechanically and thermally stable electrodes, the cathode structure should be porous to facilitate the ORR reaction [123]. Additionally, the polarization effect is important, and the pretreatment of electrodes is essential to improve the electrodes' surface area and/or hydrophilicity. The treatment of graphite felt with polyacrylonitrile (PAN-GF) or rayon (R-GF) was performed to study the effect of a precursor on the polarization effect [124]. The PAN-GF has higher conductivity due to the higher degree of graphitization, and thus more negligible ohmic polarization. Meanwhile, R-GF achieved better mass transfer and diffusion of the electrolyte on the electrode surface due to its more significant surface roughness.
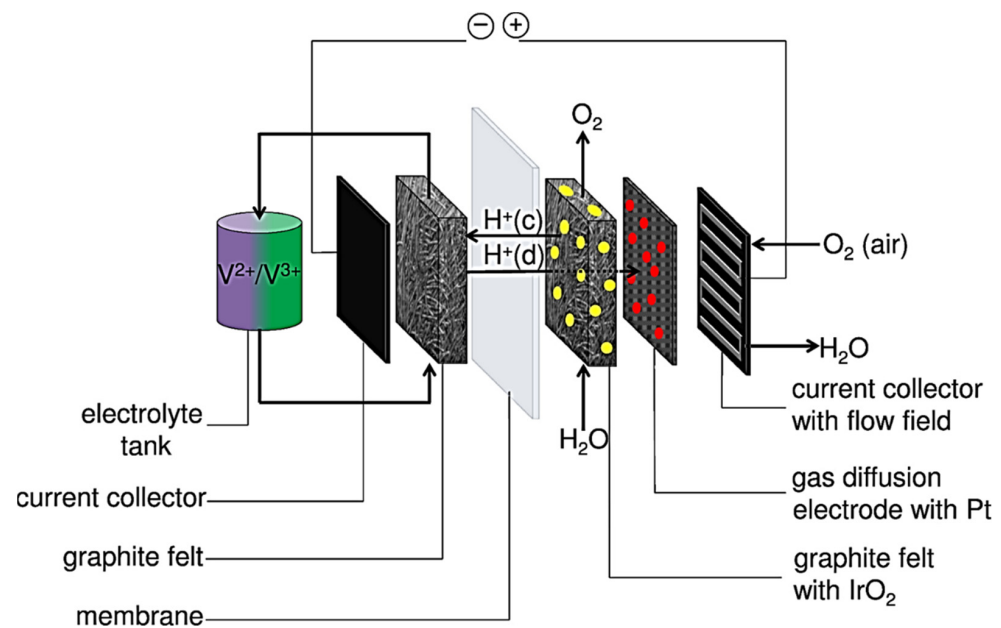

Figure 37. A bidirectional vanadium–air flow battery based on a two-layered cathode, adapted from [125].

8. Large-Scale Metal-Air Batteries

Nowadays, much concern has been given to global warming resulting from fossil fuels [126,127]. Several methods have been carried out to minimize the reliance on fossil fuels, such as using efficient energy conversion devices such as fuel cells [128–130] that are efficient and environmentally friendly [131], improving the efficiency of the current energy conversion devices and/or using renewable energy sources [132–135]. Among these different methods, renewable energy sources are the most promising option, as they are sustainable and have no or low environmental impacts [136–139]. However, the significant increase in renewable energy requires a proper energy storage system to accommodate such requirements [140,141]. With the increasing prevalence of renewable energy production sources such as wind [142–145] and solar energy [146–149], the electricity grid will need the assistance of a large-scale electrical energy storage system. The energy produced from renewable sources is intermittent, aperiodic, and changeable in nature, requiring constant attention. Consequently, storing energy during unexpected energy production periods is essential to maintain the quality of the electricity generated and satisfy the increasing electricity demand. When compared to other systems, electrochemical energy storage systems may meet the primary requirements for large-scale energy storage systems, which include a short life cycle, rapid response time, scalability, and high efficiency [84,112,150]. Electrochemical energy storage systems may also be more cost-effective than other systems. Typically, electrochemical energy storage refers to electrochemical capacitors and rechargeable batteries, which may be used in conjunction with other systems in a hybrid configuration [151,152]. For large-scale energy storage, it is necessary to have a battery with a life of 5000 charge-discharge cycles at energy efficiency of about 80% for the round trip [84].

The airflow sustains the reaction of the air electrode in the MABs, which eliminates the need for tanks to store the reactant. In addition, for the use of large-scale energy storage, the air electrode must be bifunctional for both ORR and OER during discharge and charge, respectively, in order to be effective. Because MABs are cost-effective, ultralightweight, and have a high energy density that is theoretically equal to that of gasoline, they are an excellent alternative to gasoline. In contrast, its energy efficiency is poor, and its charge/discharge life cycle is short. Figure 38 shows that MABs have a good energy density; however, the technology is still in the development stage in terms of efficiency and availability. Still, it has a possible future in the investment deferral application of distributed storage [153], as shown in the figure. It has evolved into an excellent energy storage technology for ecologically friendly and high-performance electric cars, among other applications [107]. Despite this, MABs' large-scale use is limited by their poor energy efficiency and power density, caused by a higher overpotential and slow oxygen reactions at the air cathode.
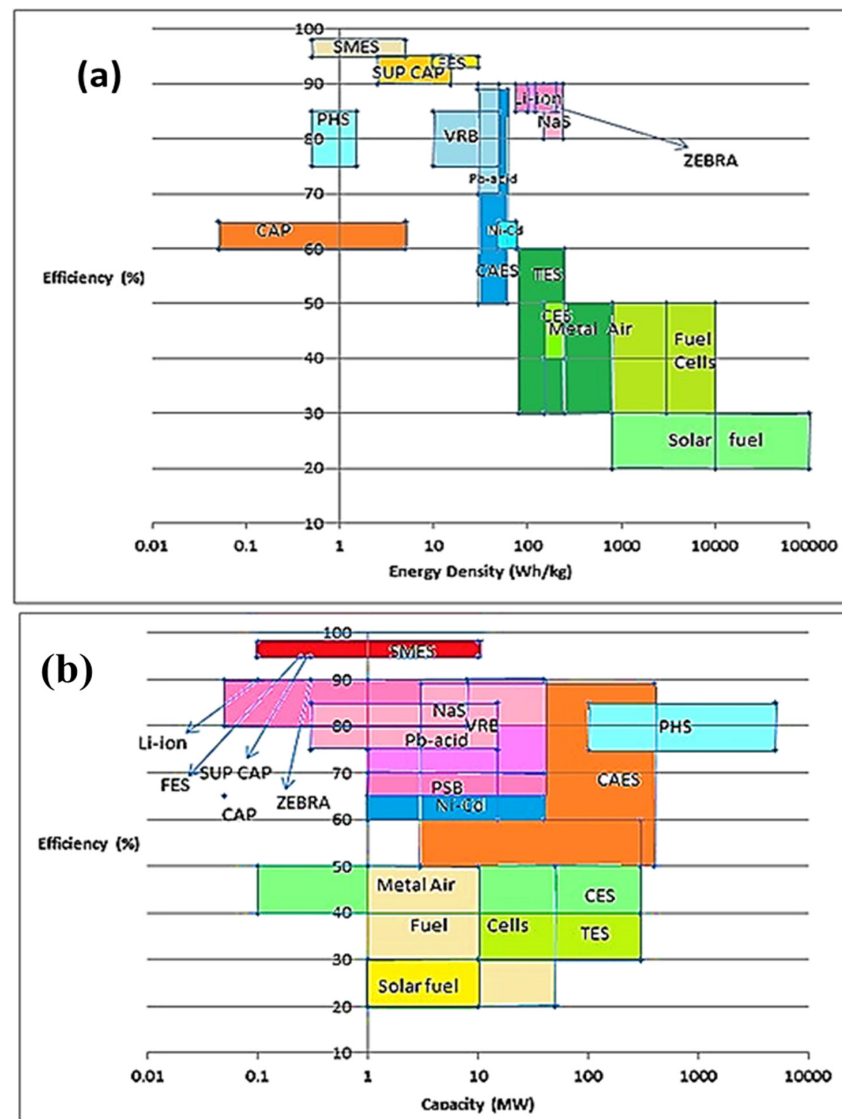
Figure 38. Round trip efficiency (**a**) vs. energy density and (**b**) vs. capacity, reproduced with permission from [153].

Iron–air batteries are a potential option for large-scale energy storage because of their cheap cost, environmental friendliness, ease of scaling up, long-term viability, and abundance of raw materials, among other characteristics. However, their cycle life and efficiency need to be improved; only then will they be a viable option [150]. Furthermore, aluminum–air batteries (AABs) have the lowest cost and the second greatest specific capacity theoretically, making them a strong prospect for large-scale energy applications in the future among MABs, particularly in renewable energy. As a result, AABs are very appealing as a sustainable and efficient technology for energy storage and conversion, with the capability of providing power for automobiles and large electronic equipment [154]. The high energy density of MABs and redox flow batteries (RFBs), as well as the unique design of their structural components, have both shown significant promise for large-scale electrical energy storage as efficient electrochemical systems. Using a combination of MABs and the idea of flow batteries to overcome side reactions results in a potential candidate for the development of a metal–air flow battery for electrical energy storage in large-scale applications. Metal–air flow technologies, because of their inherent benefits and the high degree of design freedom they provide, have tremendous potential for large-scale energy storage and transmutation in the future power grid. It is also important to note that before

contemplating the use of MAB technologies in the commercial sector, efforts should be made to ensure their safety and dependability in the industrial and academic sectors [112]. It is necessary to improve the efficiency and energy density of vanadium–air flow batteries (VAFBs) while also lowering the stack cost to be used on a large scale in commercial applications [112].

9. Applications of MABs

Metal–air batteries are used in a variety of applications. Metal–air batteries can be used as small power sources for electric cars as well as portable electronic devices. Furthermore, they may be used as energy storage devices or as effective stations of energy transfer, particularly when it comes to renewable energy producers, as they can control the flow of energy from sources such as photovoltaic (PV) panels, wind turbines, and electric grids, among other things.

9.1. Wastewater Treatment Using MABs

Besides the main function of MABs in storing energy, they can be used in the treatment of water used in the production of electricity. The studies on MABs in this area are limited or very uncommon. The study on water treatment conducted by MABs may be classified into three categories: the collection of compounds in water, the removal of heavy metals from water, and the treatment of household sewage and wastewater [87].

As a small-scale device, a MAB is simple to set up and run, and it may be used for household sewage as a pretreatment device, where it can decrease COD, total phosphorus, as well as ammonia nitrogen in domestic water to acceptable levels. When employed as a preliminary treatment unit, the high salinity of most industrial wastewater is advantageous as an electrolyte for the MAB's discharge, allowing the device to produce more products of the metal anode and, as a result, the concentration of pollutant may be reduced. At this time, only wastewater from aquaculture has been investigated [87].

Al–air and iron–air batteries from the literature have been utilized to investigate the overall efficiency of electricity production and the treatment effect of wastewater. It was discovered that higher conductivity (higher NaCl concentration) and varying pH values have little effect on the battery discharge. Higher conductivity (higher NaCl concentration) and different pH values have little impact on the battery discharge. Furthermore, it was highlighted that an aluminum–iron double anode exhibited the best battery efficiency [87–89].

As shown in Figure 39, an aluminum-air battery (AAB) was coupled with a microbial electrolysis cell MEC to produce hydrogen, clean wastewater, and generate coagulants, all without the need for external energy. Both contribute to energy recovery as a result of this combination. It has been shown that the Al–air battery-MEC system is self-sufficient in terms of energy supply, with an AAB of 28 mL providing 0.58 to 0.8 volts of electricity for an MEC of 28 Ml [89].
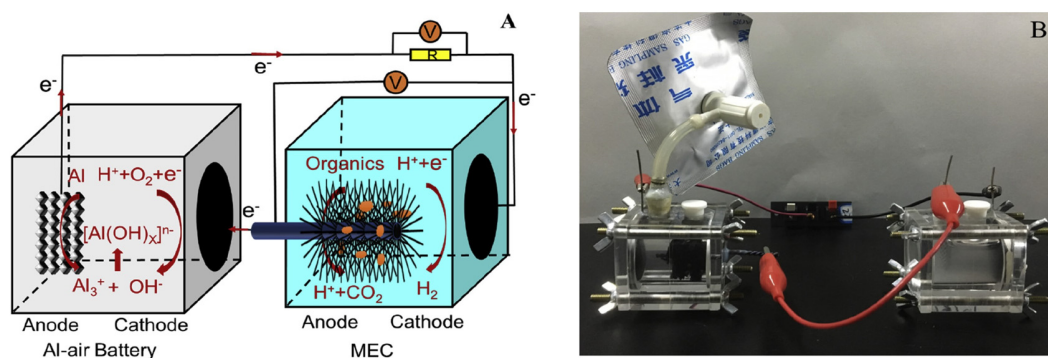

Figure 39. (**A**) Schematic diagram and (**B**) photograph of the MEC and AAB combined system, with permission to reproduce from [89].

9.2. Water Desalination Using MABs

Because the process of generating fresh water consumes energy, water desalination necessitates the development of high-performance as well as low-energy technologies. In addition to their capacity to store energy, electrochemical methods hold tremendous prospects for the desalination of water [155–158]. A metal-air desalination battery (MADB) is a device that can desalinate water while also generating energy. It is self-powered and has the capability of generating electricity. As shown in Figure 40, the MADB included an AAB that used seawater as both a desalination solution and an electrolyte. The effectiveness of the MADB idea is demonstrated by the desalination performance, stability, and power output that have been achieved. However, the amount of energy produced and the pace of desalination were both restricted by the quantity of dissolved oxygen in the cathode. The highest power density achieved was 2.83 W m^{-2} at a current density of 6.58 A m^{-2} and an output voltage of 0.43 V, with the current density being 6.58 A m^{-2} and the output voltage being 0.43 V. Additionally, it reduces salinity by 37.8 percent while generating 10 mW h of energy for 14 h of operation. Further development of the MADB may make it possible to use this idea in the future in actual applications on a large or small scale [159].
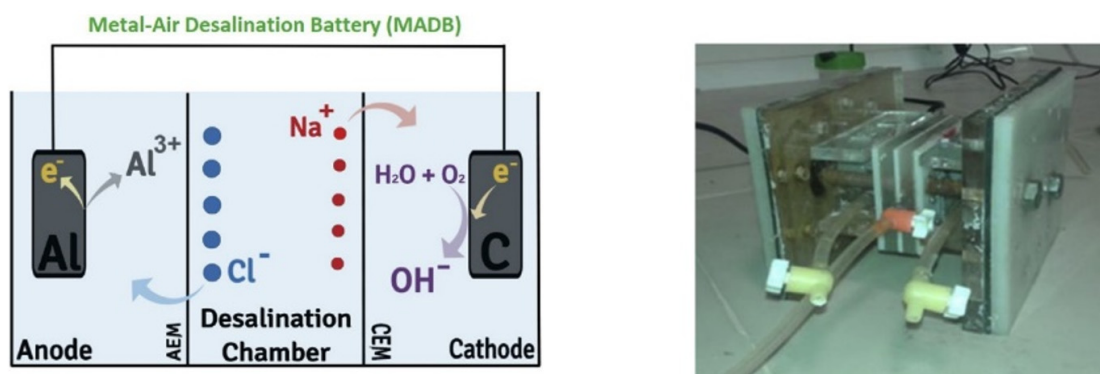

Figure 40. Schematic diagram of the MADB's three-chamber cell on the left side and a photograph on the right side, with permission to reproduce from [159].

Zinc-air desalination (ZAD) in Figure 41 has been utilized from the literature for electrochemical desalination using MAB technology. The ZAD cell using MoS$_2$ bifunctional catalyst showed a 0.9 to 1.0 mg NaCl/cm^2 desalination capacity and 70% charge efficiency at a current density of 1 mA/cm^2. The metal-air desalination MAD is a new technology that provides a highly promising performance for electrochemical desalination based on non-noble metal catalysts [156].

An aluminum-air battery (AAB) was combined with an electrodialysis system. The membrane of the AAB was replaced with the electrodialysis cell to decrease the amount of energy needed for water desalination. The desalination occurs in the middle chamber in a three-chamber system, which is separated by cation and anion exchange membranes (CEM and AEM, respectively) from the side chambers. The anode and cathode electrochemical reactions provide a sufficient driving force: an electro-osmotic drag force for ion diffusion from sea salt water into anode and cathode chambers. The integrated system using an electrolyte of NaOH 5 mM produced an open-circuit voltage of 1.6 V at a current density of 3 mA/cm^2 during one hour of cell operation, the saltwater conductivity decreased from 5 to 4 ms, indicating the decrease in the number of ions in the water. The cell produced 4.8 mW/cm^2 of power. This combined system can work without requiring any power source [160]. A Zn–air battery with N-doped porous carbon (NPC) as an electrocatalyst for ORR was also utilized as a power source for capacitive deionization CDI, which demonstrated excellent desalination performance when NPC was functionalized with sulfuric acid as the CDI cathode material [23,161].
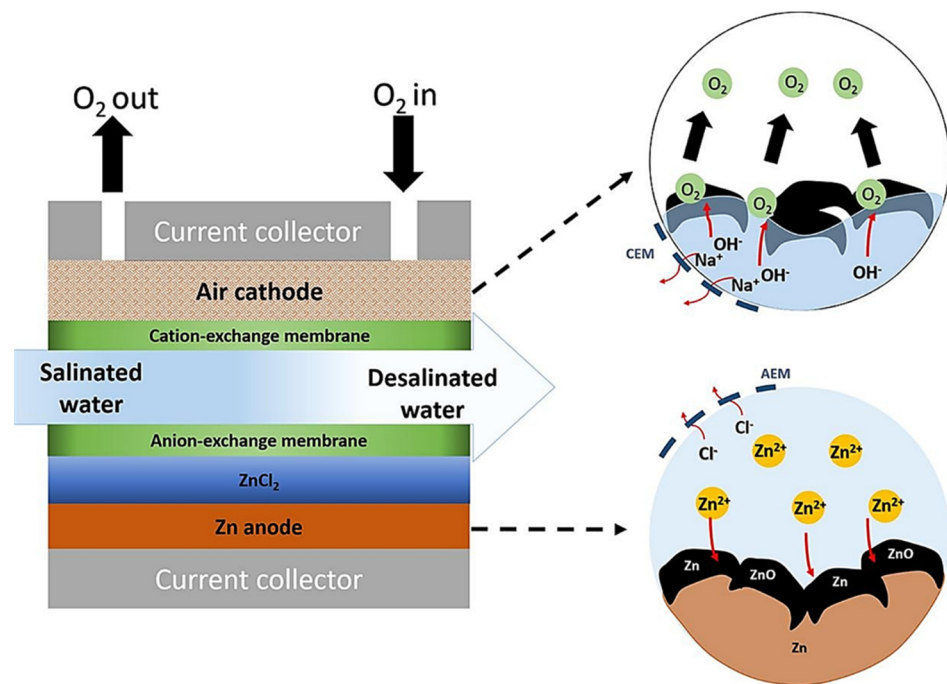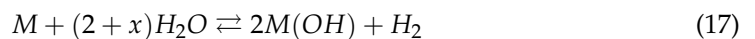
Figure 41. Configuration of Zn–air desalination ZAD cell, adapted from [156].

10. Challenges of MABs

Although the MAB technology has been researched over the last decade, several technical difficulties must be solved before the concept can be commercially implemented.

10.1. Metallic Anode Challenges

One of the critical problems facing MABs is the corrosion, passivation, and dendritic formation of the metallic anode. Corrosion is one of the most crucial side reactions between a metal and an electrolyte, as shown by the following process.

$$M + (2+x)H_2O \rightleftharpoons 2M(OH) + H_2 \tag{17}$$

$$M + H_2O \rightleftharpoons MO_X + H_2 \tag{18}$$

Hydrogen evolution is naturally favored in nearly all MABs because the standard voltage of M/MO is below the level of hydrogen evolution. The rate of corrosion caused by the hydrogen evolution reaction (HER) may be calculated using the equations above. The HER can decrease the columbic efficiency of a metal anode, which may result in a battery explosion. Corrosion may occur in FABs, AABs, ZABs, and LABs, among other types of batteries. Table 12 illustrates several methods for lowering the HER rate while simultaneously increasing charging efficiency.

Table 12. Reducing corrosion strategies [16].

Metal	Reducing Corrosion or HER Rate by
ZnO surface	Increasing ZnO reduces the self-discharge rate.
Al	Changing purity, properties, and temperature of the alkaline electrolyte. Utilization of ionic membrane.
Fe	Using an alloy as an anode instead of pure metal and additives such as sulfur or bismuth is a good way to save money.

Passivation is the development of an insulating layer on the electrode surface, which prevents the discharge product from moving around. Electrode discharge is prevented by

the layer that develops. This may be found in AABs, ZABs, and LABs batteries, among other things. Depending on the system, the passivation layers in MABs are LiOH, ZnO, and Al_2O_3, respectively. In the presence of an air cathode, the generated soluble species turned to a non-conductive layer on the surface of the metal. They raise the cell's internal electric resistance, which prevents the dissolving of metal. Using porous electrodes to avoid the development of a passivation layer is an effective approach [16].

Dendritic formation and deformation cause the shape of the metal electrode to gradually change, meaning that the surface roughness becomes uneven as dendrites form. This occurs due to the accumulation of metal ions during metal electrode cycling in alkaline electrolytes. This can result in an unstable battery system, or it may cause a shortcut. Dendritic structures form in Li-air, Fe-air, and Zn-air batteries [16].

10.2. Electrolyte Challenges

Dissolving CO_2 from the air in the aqueous KOH electrolyte represents a challenge for some types of MABs, such as ZABs, because CO_2 reacts with OH^- and forms CO_3^{2-}, thus reducing the electrolyte conductivity and slowing the cell reaction down. Appling a CO_2 filter could solve this problem, but it will increase the complexity and the cost of the system [23].

The evolution of hydrogen gas could be a challenge for electrolytes with a metal electrode with a lower potential than hydrogen evolution because the electrolyte becomes thermodynamically unstable [23]. When using an active electrolyte, the insoluble by-products' deposition on both electrodes' surfaces during the charge-discharge cycles is a challenge that must be taken into consideration. These by-products reduce the battery's performance due to blocking the electrode pores, limiting air diffusion [16,162].

The absorption of moisture from the environment and the evaporation of electrolytes both contribute to the shortening of the life of aqueous MABs. As a result of the accumulation of water, air electrode flooding may occur, which may impair oxygen delivery to the active areas of the catalyst. However, water loss raises the electrolyte concentration in the body, which has a detrimental impact on the discharge response. Additionally, if the electrolyte is diluted, the ionic conductivity will be decreased, resulting in higher internal resistances in the system. When designing the battery, it is possible to optimize the internal water balance by considering the quantity of metal used, the composition and volume of the electrolyte, and the degree of gas diffusion. The polymerization of the electrolyte may help to decrease the amount of moisture that is lost. Furthermore, the use of a siloxane membrane protects against flooding and drying out [87].

10.3. Cathode Challenges

It is challenging to develop a bi-functional air catalyst that is stable, active, and inexpensive and is appropriate for both OER and ORR [23]. The precipitation of solid products such as Li_2O_2 in the cathode results in a thick layer that inhibits electron transport and may even result in the blocking of cathode pores, reducing the overall capacity of the cell. The transfer of oxygen is a problem for certain types of MAB when operating at high current densities [23].

11. Conclusions

Metal–air batteries are promising electrochemical devices with a high energy density that are safe, environmentally friendly, and lightweight. MABs have a wide range of applications, including portable electric devices, wearable devices, and large-scale applications, such as electric cars, among many others. This work thoroughly discusses the mechanism of MABs, types, electrode materials, electrolytes, new designs, and new applications. The challenges and recommendations are given.

The following conclusions are driven:

- Various metals can be used as an anode of MABs. Each metal has its own advantages and disadvantages. Al is one of the promising electrodes due to its high energy density, low weight, good recyclability, environmental friendliness, and low cost.
- Despite the high ionic conductivity of the aqueous electrolytes, the leakage, stability, and thermodynamic limitations are challenges facing their application. Electrolyte additives or non-aqueous electrolytes can minimize or solve these problems and thus increase the durability and energy density of MABs.
- A thermally and mechanically porous cathode electrode that can perform ORR and OER effectively is essential for commercial MABs.
- Both the Al-air batteries and iron–air batteries are good candidates for the large-scale production of MABs
- Flow MABs are safe and have a long operational life because of the flow of anolyte/electrolyte, which minimizes side reactions. Flow MABs can be used for large-scale energy storage as well as stationary power plants.
- A few studies conducted on MABs in water desalination and wastewater treatment have shown promising results. However, more studies are still required.

References

1. Berger, R. Focus: Business Models in Energy Storage. Available online: https://www.rolandberger.com/publications/publication_pdf/roland_berger_energy_storage_final.pdf. (accessed on 12 August 2021).
2. Zhang, H.; Sun, C. Cost-effective iron-based aqueous redox flow batteries for large-scale energy storage application: A review. *J. Power Sources* **2021**, *493*, 229445. [CrossRef]
3. Zhang, H.; Chen, N.; Sun, C.; Luo, X. Investigations on physicochemical properties and electrochemical performance of graphite felt and carbon felt for iron-chromium redox flow battery. *Int. J. Energy Res.* **2020**, *44*, 3839–3853. [CrossRef]
4. Zablocki, A. Fact Sheet | Energy Storage. Available online: https://www.eesi.org/papers/view/energy-storage-2019 (accessed on 1 October 2021).
5. Olabi, A.G.; Onumaegbu, C.; Wilberforce, T.; Ramadan, M.; Abdelkareem, M.A.; Al–Alami, A.H. Critical review of energy storage systems. *Energy* **2021**, *214*, 118987. [CrossRef]
6. Zhang, D.; Zhao, H.; Liang, F.; Ma, W.; Lei, Y. Nanostructured arrays for metal–ion battery and metal–air battery applications. *J. Power Sources* **2021**, *493*, 229722. [CrossRef]
7. Chen, X.; Ali, I.; Song, L.; Song, P.; Zhang, Y.; Maria, S.; Nazmus, S.; Yang, W.; Dhakal, H.N.; Li, H. A review on recent advancement of nano-structured-fiber-based metal-air batteries and future perspective. *Renew. Sustain. Energy Rev.* **2020**, *134*, 110085. [CrossRef]
8. Kumar, P.; Goyal, S.K.; Singh, B.P. Application of bifunctional catalysts and metal organic frameworks in metal air batteries for renewable power conversion applications. *Mater. Today Proc.* **2021**, *43*, 2839–2842. [CrossRef]
9. Cai, W.; Deng, J.; Lu, H.; Cao, Y. Performance of metal borides as anode in metal boride-air battery. *Mater. Chem. Phys.* **2020**, *251*, 123101. [CrossRef]
10. Mladenova, E.; Slavova, M.; Mihaylova-Dimitrova, E.; Burdin, B.; Abrashev, B.; Krapchanska, M.; Raikova, G.; Vladikova, D. Monolithic carbon-free gas diffusion electrodes for secondary metal-air batteries. *J. Electroanal. Chem.* **2021**, *887*, 115112. [CrossRef]
11. Gauthier, M.; Nguyen, M.H.; Blondeau, L.; Foy, E.; Wong, A. Operando NMR characterization of a metal-air battery using a double-compartment cell design. *Solid State Nucl. Magn. Reson.* **2021**, *113*, 101731. [CrossRef]

12. Bo, W.; Ahmad, Z.; Alanzi, A.R.A.; Al-Omari, A.I.; Hafez, E.H.; Abdelwahab, S.F. The Current COVID-19 Pandemic in China: An Overview and Corona Data Analysis. *Alex. Eng. J.* **2021**. [CrossRef]

13. Liu, Q.; Pan, Z.; Wang, E.; An, L.; Sun, G. Aqueous metal-air batteries: Fundamentals and applications. *Energy Storage Mater.* **2020**, *27*, 478–505. [CrossRef]

14. Nagy, T.; Nagy, L.; Erdélyi, Z.; Baradács, E.; Deák, G.; Zsuga, M.; Kéki, S. Environmentally friendly Zn-air rechargeable battery with heavy metal free charcoal based air cathode. *Electrochim. Acta* **2021**, *368*, 137592. [CrossRef]

15. Marini, E.; Jörissen, L.; Brimaud, S. Rational design of a low-cost, durable and efficient bifunctional oxygen electrode for rechargeable metal-air batteries. *J. Power Sources* **2021**, *482*, 228900. [CrossRef]

16. Wang, C.; Yu, Y.; Niu, J.; Liu, Y.; Bridges, D.; Liu, X.; Pooran, J.; Zhang, Y.; Hu, A. Recent progress of metal–air batteries—A mini review. *Appl. Sci.* **2019**, *9*, 2787. [CrossRef]

17. Hannan, M.A.; Lipu, M.S.H.; Hussain, A.; Mohamed, A. A review of lithium-ion battery state of charge estimation and management system in electric vehicle applications: Challenges and recommendations. *Renew. Sustain. Energy Rev.* **2017**, *78*, 834–854. [CrossRef]

18. Li, J.; Du, Z.; Ruther, R.E.; An, S.J.; David, L.A.; Hays, K.; Wood, M.; Phillip, N.D.; Sheng, Y.; Mao, C. Toward low-cost, high-energy density, and high-power density lithium-ion batteries. *Jom* **2017**, *69*, 1484–1496. [CrossRef]

19. Clemente, A.; Costa-Castelló, R. Redox flow batteries: A literature review oriented to automatic control. *Energies* **2020**, *13*, 4514. [CrossRef]

20. Lopes, P.P.; Stamenkovic, V.R. Past, present, and future of lead–acid batteries. *Science* **2020**, *369*, 923–924. [CrossRef]

21. Cheng, Y.; Wang, X.; Huang, S.; Samarakoon, W.; Xi, S.; Ji, Y.; Zhang, H.; Zhang, F.; Du, Y.; Feng, Z. Redox targeting-based vanadium redox-flow battery. *ACS Energy Lett.* **2019**, *4*, 3028–3035. [CrossRef]

22. Zhang, Z.H.; Wei, L.; Wu, M.C.; Bai, B.F.; Zhao, T.S. Chloride ions as an electrolyte additive for high performance vanadium redox flow batteries. *Appl. Energy* **2021**, *289*, 116690. [CrossRef]

23. Clark, S.; Latz, A.; Horstmann, B. A review of model-based design tools for metal-air batteries. *Batteries* **2018**, *4*, 5. [CrossRef]

24. Gröger, O.; Gasteiger, H.A.; Suchsland, J.-P. Erratum: Review—Electromobility: Batteries or Fuel Cells? [J. Electrochem. Soc., 162, A2605 (2015)]. *J. Electrochem. Soc.* **2016**, *163*, X3. [CrossRef]

25. Rahman, M.A.; Wang, X.; Wen, C. High energy density metal-air batteries: A review. *J. Electrochem. Soc.* **2013**, *160*, A1759. [CrossRef]

26. Zhang, T.; Tao, Z.; Chen, J. Magnesium–air batteries: From principle to application. *Mater. Horiz.* **2014**, *1*, 196–206. [CrossRef]

27. Li, Y.; Zhang, X.; Li, H.-B.; Yoo, H.D.; Chi, X.; An, Q.; Liu, J.; Yu, M.; Wang, W.; Yao, Y. Mixed-phase mullite electrocatalyst for pH-neutral oxygen reduction in magnesium-air batteries. *Nano Energy* **2016**, *27*, 8–16. [CrossRef]

28. Li, C.S.; Sun, Y.; Gebert, F.; Chou, S.L. Current progress on rechargeable magnesium–air battery. *Adv. Energy Mater.* **2017**, *7*, 1700869. [CrossRef]

29. Zhang, Z.; Zuo, C.; Liu, Z.; Yu, Y.; Zuo, Y.; Song, Y. All-solid-state Al–air batteries with polymer alkaline gel electrolyte. *J. Power Sources* **2014**, *251*, 470–475. [CrossRef]

30. Liu, X.; Zhang, P.; Xue, J.; Zhu, C.; Li, X.; Wang, Z. High energy efficiency of Al-based anodes for Al-air battery by simultaneous addition of Mn and Sb. *Chem. Eng. J.* **2021**, *417*, 128006. [CrossRef]

31. Mokhtar, M.; Talib, M.Z.M.; Majlan, E.H.; Tasirin, S.M.; Ramli, W.M.F.W.; Daud, W.R.W.; Sahari, J. Recent developments in materials for aluminum–air batteries: A review. *J. Ind. Eng. Chem.* **2015**, *32*, 1–20. [CrossRef]

32. Bi, X.; Wang, R.; Yuan, Y.; Zhang, D.; Zhang, T.; Ma, L.; Lu, J. From sodium–oxygen to sodium–air battery: Enabled by sodium peroxide dihydrate. *Nano Lett.* **2020**, *20*, 4681–4686. [CrossRef]

33. Sahgong, S.H.; Senthilkumar, S.T.; Kim, K.; Hwang, S.M.; Kim, Y. Rechargeable aqueous Na–air batteries: Highly improved voltage efficiency by use of catalysts. *Electrochem. Commun.* **2015**, *61*, 53–56. [CrossRef]

34. Adelhelm, P.; Hartmann, P.; Bender, C.L.; Busche, M.; Eufinger, C.; Janek, J. From lithium to sodium: Cell chemistry of room temperature sodium–air and sodium–sulfur batteries. *Beilstein J. Nanotechnol.* **2015**, *6*, 1016–1055. [CrossRef]

35. Bansal, R.; Menon, P.; Sharma, R.C. Silicon–air batteries: Progress, applications and challenges. *SN Appl. Sci.* **2020**, *2*, 1–17. [CrossRef]

36. Leong, K.W.; Wang, Y.; Ni, M.; Pan, W.; Luo, S.; Leung, D.Y. Rechargeable Zn-air batteries: Recent trends and future perspectives. *Renew. Sustain. Energy Rev.* **2022**, *154*, 111771. [CrossRef]

37. Girishkumar, G.; McCloskey, B.; Luntz, A.C.; Swanson, S.; Wilcke, W. Lithium− air battery: Promise and challenges. *J. Phys. Chem. Lett.* **2010**, *1*, 2193–2203. [CrossRef]

38. Blurton, K.F.; Sammells, A.F. Metal/air batteries: Their status and potential—A review. *J. Power Sources* **1979**, *4*, 263–279. [CrossRef]

39. Abraham, K.; Jiang, Z. A polymer electrolyte-based rechargeable lithium/oxygen battery. *J. Electrochem. Soc.* **1996**, *143*, 1. [CrossRef]

40. McCloskey, B.; Speidel, A.; Scheffler, R.; Miller, D.; Viswanathan, V.; Hummelshøj, J.; Nørskov, J.; Luntz, A. Twin problems of interfacial carbonate formation in nonaqueous Li–O2 batteries. *J. Phys. Chem. Lett.* **2012**, *3*, 997–1001. [CrossRef]

41. Monroe, C.W. Does oxygen transport affect the cell voltages of metal/air batteries? *J. Electrochem. Soc.* **2017**, *164*, E3547. [CrossRef]

42. Horstmann, B.; Danner, T.; Bessler, W.G. Precipitation in aqueous lithium–oxygen batteries: A model-based analysis. *Energy Environ. Sci.* **2013**, *6*, 1299–1314. [CrossRef]

43. Danner, T.; Horstmann, B.; Wittmaier, D.; Wagner, N.; Bessler, W.G. Reaction and transport in Ag/Ag$_2$O gas diffusion electrodes of aqueous Li–O2 batteries: Experiments and modeling. *J. Power Sources* **2014**, *264*, 320–332. [CrossRef]

44. Vegge, T.; Garcia-Lastra, J.M.; Siegel, D.J. Lithium–oxygen batteries: At a crossroads? *Curr. Opin. Electrochem.* **2017**, *6*, 100–107. [CrossRef]

45. Pei, P.; Wang, K.; Ma, Z. Technologies for extending zinc–air battery's cyclelife: A review. *Appl. Energy* **2014**, *128*, 315–324. [CrossRef]

46. Sumboja, A.; Ge, X.; Zheng, G.; Goh, F.T.; Hor, T.A.; Zong, Y.; Liu, Z. Durable rechargeable zinc-air batteries with neutral electrolyte and manganese oxide catalyst. *J. Power Sources* **2016**, *332*, 330–336. [CrossRef]

47. Friesen, C.A.; Krishnan, R.; Friesen, G. Rechargeable Electrochemical Cell System with a Charging Electrode Charge/Discharge Mode Switching in the Cells. U.S. Patent Application No. 12/885,268, 24 March 2011.

48. Liu, Q.; Chang, Z.; Li, Z.; Zhang, X. Flexible metal–air batteries: Progress, challenges, and perspectives. *Small Methods* **2018**, *2*, 1700231. [CrossRef]

49. Zhang, X.-b. *Metal-Air Batteries: Fundamentals and Applications*; John Wiley & Sons: Hoboken, NJ, USA, 2018.

50. Durmus, Y.E.; Zhang, H.; Baakes, F.; Desmaizieres, G.; Hayun, H.; Yang, L.; Kolek, M.; Küpers, V.; Janek, J.; Mandler, D.; et al. Side by Side Battery Technologies with Lithium-Ion Based Batteries. *Adv. Energy Mater.* **2020**, *10*, 2000089. [CrossRef]

51. McKerracher, R.; de Ponce Leon, C.; Wills, R.; Shah, A.; Walsh, F.C. A review of the iron–air secondary battery for energy storage. *ChemPlusChem* **2015**, *80*, 323–335. [CrossRef]

52. Li, Y.; Dai, H. Recent advances in zinc–air batteries. *Chem. Soc. Rev.* **2014**, *43*, 5257–5275. [CrossRef]

53. Gür, T.M. Review of electrical energy storage technologies, materials and systems: Challenges and prospects for large-scale grid storage. *Energy Environ. Sci.* **2018**, *11*, 2696–2767. [CrossRef]

54. Komilis, D.; Evangelou, A.; Giannakis, G.; Lymperis, C. Revisiting the elemental composition and the calorific value of the organic fraction of municipal solid wastes. *Waste Manag.* **2012**, *32*, 372–381. [CrossRef] [PubMed]

55. Gesser, H. Electrochemistry, Batteries and Fuel Cells. In *Applied Chemistry*; Springer: Berlin/Heidelberg, Germany, 2002; pp. 159–190.

56. Yoshio, M.; Brodd, R.J.; Kozawa, A. *Lithium-Ion Batteries*; Springer: New York, NY, USA, 2009; Volume 1, pp. 2–3.

57. Kang, J.; Yan, F.; Zhang, P.; Du, C. A novel way to calculate energy efficiency for rechargeable batteries. *J. Power Sources* **2012**, *206*, 310–314. [CrossRef]

58. Weinrich, H.; Durmus, Y.E.; Tempel, H.; Kungl, H.; Eichel, R.-A. Silicon and iron as resource-efficient anode materials for ambient-temperature metal-air batteries: A review. *Materials* **2019**, *12*, 2134. [CrossRef] [PubMed]

59. Khan, Z.; Parveen, N.; Ansari, S.A.; Senthilkumar, S.; Park, S.; Kim, Y.; Cho, M.H.; Ko, H. Three-dimensional SnS2 nanopetals for hybrid sodium-air batteries. *Electrochim. Acta* **2017**, *257*, 328–334. [CrossRef]

60. Liu, Y.; Sun, Q.; Yang, X.; Liang, J.; Wang, B.; Koo, A.; Li, R.; Li, J.; Sun, X. High-performance and recyclable Al-air coin cells based on eco-friendly chitosan hydrogel membranes. *ACS Appl. Mater. Interfaces* **2018**, *10*, 19730–19738. [CrossRef] [PubMed]

61. Zhao, Y.; Huang, G.; Zhang, C.; Peng, C.; Pan, F. Effect of phosphate and vanadate as electrolyte additives on the performance of Mg-air batteries. *Mater. Chem. Phys.* **2018**, *218*, 256–261. [CrossRef]

62. Chen, G.; Zhang, J.; Wang, F.; Wang, L.; Liao, Z.; Zschech, E.; Müllen, K.; Feng, X. Cobalt-Based Metal–Organic Framework Nanoarrays as Bifunctional Oxygen Electrocatalysts for Rechargeable Zn-Air Batteries. *Chem. A Eur. J.* **2018**, *24*, 18413–18418. [CrossRef] [PubMed]

63. Lai, C.; Wang, J.; Lei, W.; Xuan, C.; Xiao, W.; Zhao, T.; Huang, T.; Chen, L.; Zhu, Y.; Wang, D. Restricting growth of Ni$_3$Fe nanoparticles on heteroatom-doped carbon nanotube/graphene nanosheets as air-electrode electrocatalyst for Zn–air battery. *ACS Appl. Mater. Interfaces* **2018**, *10*, 38093–38100. [CrossRef]

64. Figueredo-Rodríguez, H.; McKerracher, R.; Insausti, M.; Luis, A.G.; de León, C.P.; Alegre, C.; Baglio, V.; Aricò, A.; Walsh, F. A rechargeable, aqueous iron air battery with nanostructured electrodes capable of high energy density operation. *J. Electrochem. Soc.* **2017**, *164*, A1148. [CrossRef]

65. Sumathi, S.; Sethuprakash, V.; Basirun, W.; Zainol, I.; Sookhakian, M. Polyacrylamide-methanesulfonic acid gel polymer electrolytes for tin-air battery. *J. Sol-Gel Sci. Technol.* **2014**, *69*, 480–487. [CrossRef]

66. Najam, T.; Shah, S.S.A.; Ding, W.; Deng, J.; Wei, Z. Enhancing by nano-engineering: Hierarchical architectures as oxygen reduction/evolution reactions for zinc-air batteries. *J. Power Sources* **2019**, *438*, 226919. [CrossRef]

67. Egan, D.R.; Ponce de León, C.; Wood, R.J.K.; Jones, R.L.; Stokes, K.R.; Walsh, F.C. Developments in electrode materials and electrolytes for aluminium–air batteries. *J. Power Sources* **2013**, *236*, 293–310. [CrossRef]

68. Mutlu, R.N.; Ateş, Ş.; Yazıcı, B. Al-6013-T6 and Al-7075-T7351 alloy anodes for aluminium-air battery. *Int. J. Hydrogen Energy* **2017**, *42*, 23315–23325. [CrossRef]

69. Chawla, N. Recent advances in air-battery chemistries. *Mater. Today Chem.* **2019**, *12*, 324–331. [CrossRef]

70. Melhem, Z. *Electricity Transmission, Distribution and Storage Systems*; Woodhead Publishing Series in Energy: Number 38; Woodhead Publishing: Shaxton, UK, 2013.

71. Imanishi, N.; Yamamoto, O. Perspectives and challenges of rechargeable lithium–air batteries. *Mater. Today Adv.* **2019**, *4*, 100031. [CrossRef]

72. Rahman, M.A.; Wang, X.; Wen, C. A review of high energy density lithium–air battery technology. *J. Appl. Electrochem.* **2014**, *44*, 5–22. [CrossRef]

73. Lin, H.; Chen, Z.; Wang, D.; Wang, M.; Peng, Z.; Liu, Z.; He, H.; Wang, M.; Li, H. High-performance Li-air battery after limiting inter-electrode crosstalk. *Energy Storage Mater.* **2021**, *39*, 225–231. [CrossRef]

74. Otaegui, L.; Rodriguez-Martinez, L.M.; Wang, L.; Laresgoiti, A.; Tsukamoto, H.; Han, M.H.; Tsai, C.L.; Laresgoiti, I.; López, C.M.; Rojo, T. Performance and stability of a liquid anode high-temperature metal–air battery. *J. Power Sources* **2014**, *247*, 749–755. [CrossRef]

75. Wang, H.-F.; Xu, Q. Materials design for rechargeable metal-air batteries. *Matter* **2019**, *1*, 565–595. [CrossRef]

76. Jung, K.-N.; Kim, J.; Yamauchi, Y.; Park, M.-S.; Lee, J.-W.; Kim, J.H. Rechargeable lithium–air batteries: A perspective on the development of oxygen electrodes. *J. Mater. Chem. A* **2016**, *4*, 14050–14068. [CrossRef]

77. Christensen, J.; Albertus, P.; Sanchez-Carrera, R.S.; Lohmann, T.; Kozinsky, B.; Liedtke, R.; Ahmed, J.; Kojic, A. A critical review of Li/air batteries. *J. Electrochem. Soc.* **2011**, *159*, R1. [CrossRef]

78. Gelman, D.; Shvartsev, B.; Ein-Eli, Y. Aluminum–air battery based on an ionic liquid electrolyte. *J. Mater. Chem. A* **2014**, *2*, 20237–20242. [CrossRef]

79. Cohn, G.; Ein-Eli, Y. Study and development of non-aqueous silicon-air battery. *J. Power Sources* **2010**, *195*, 4963–4970. [CrossRef]

80. Durmus, Y.E.; Aslanbas, Ö.; Kayser, S.; Tempel, H.; Hausen, F.; De Haart, L.; Granwehr, J.; Ein-Eli, Y.; Eichel, R.-A.; Kungl, H. Long run discharge, performance and efficiency of primary Silicon–air cells with alkaline electrolyte. *Electrochim. Acta* **2017**, *225*, 215–224. [CrossRef]

81. Reinsberg, P.; Bondue, C.J.; Baltruschat, H. Calcium–Oxygen Batteries as a Promising Alternative to Sodium–Oxygen Batteries. *J. Phys. Chem. C* **2016**, *120*, 22179–22185. [CrossRef]

82. Shiga, T.; Hase, Y.; Kato, Y.; Inoue, M.; Takechi, K. A rechargeable non-aqueous Mg–O_2 battery. *Chem. Commun.* **2013**, *49*, 9152–9154. [CrossRef] [PubMed]

83. Das, S.K.; Lau, S.; Archer, L.A. Sodium–oxygen batteries: A new class of metal–air batteries. *J. Mater. Chem. A* **2014**, *2*, 12623–12629. [CrossRef]

84. Narayanan, S.R.; Prakash, G.K.S.; Manohar, A.; Yang, B.; Malkhandi, S.; Kindler, A. Materials challenges and technical approaches for realizing inexpensive and robust iron–air batteries for large-scale energy storage. *Solid State Ion.* **2012**, *216*, 105–109. [CrossRef]

85. Ren, X.; Wu, Y. A low-overpotential potassium–oxygen battery based on potassium superoxide. *J. Am. Chem. Soc.* **2013**, *135*, 2923–2926. [CrossRef] [PubMed]

86. Dincer, I. *Comprehensive Energy Systems*; Elsevier: Amsterdam, The Netherlands, 2018.

87. Wei, W.; Xu, Y.; Huang, J.; Zhu, J. Review of the application of metal-air battery principle in water treatment. In Proceedings of the 2019 International Conference on Building Energy Conservation, Thermal Safety and Environmental Pollution Control, Hefei, China, 1–3 November 2019; p. 06035.

88. Han, X.; Qu, Y.; Li, D.; Dong, Y.; Chen, D.; Yu, Y.; Ren, N.; Feng, Y. Combined microbial electrolysis cell–iron-air battery system for hydrogen production and swine wastewater treatment. *Process Biochem.* **2021**, *101*, 104–110. [CrossRef]

89. Han, X.; Qu, Y.; Dong, Y.; Zhao, J.; Jia, L.; Yu, Y.; Zhang, P.; Li, D.; Ren, N.; Feng, Y. Microbial electrolysis cell powered by an aluminum-air battery for hydrogen generation, in-situ coagulant production and wastewater treatment. *Int. J. Hydrog. Energy* **2018**, *43*, 7764–7772. [CrossRef]

90. Demir-Cakan, R.; Palacin, M.R.; Croguennec, L. Rechargeable aqueous electrolyte batteries: From univalent to multivalent cation chemistry. *J. Mater. Chem. A* **2019**, *7*, 20519–20539. [CrossRef]

91. Mori, R. Recent developments for aluminum–air batteries. *Electrochem. Energy Rev.* **2020**, *3*, 344–369. [CrossRef]

92. Kar, M.; Simons, T.J.; Forsyth, M.; MacFarlane, D.R. Ionic liquid electrolytes as a platform for rechargeable metal–air batteries: A perspective. *Phys. Chem. Chem. Phys.* **2014**, *16*, 18658–18674. [CrossRef]

93. Khan, Z.; Vagin, M.; Crispin, X. Can hybrid Na–air batteries outperform nonaqueous Na–O2 batteries? *Adv. Sci.* **2020**, *7*, 1902866. [CrossRef] [PubMed]

94. Yu, X.; Manthiram, A. A voltage-enhanced, low-cost aqueous iron–air battery enabled with a mediator-ion solid electrolyte. *ACS Energy Lett.* **2017**, *2*, 1050–1055. [CrossRef]

95. No More Trial-and Error When Choosing an Electrolyte for Metal-Air Batteries. Available online: https://phys.org/news/2019-07-trial-and-error-electrolyte-metal-air-batteries.html (accessed on 7 May 2021).

96. Sankarasubramanian, S.; Kahky, J.; Ramani, V. Tuning anion solvation energetics enhances potassium–oxygen battery performance. *Proc. Natl. Acad. Sci. USA* **2019**, *116*, 14899–14904. [CrossRef]

97. Mainar, A.R.; Iruin, E.; Colmenares, L.C.; Kvasha, A.; De Meatza, I.; Bengoechea, M.; Leonet, O.; Boyano, I.; Zhang, Z.; Blazquez, J.A. An overview of progress in electrolytes for secondary zinc-air batteries and other storage systems based on zinc. *J. Energy Storage* **2018**, *15*, 304–328. [CrossRef]

98. Zha, Z.; Shen, C.; Wang, D.; Han, W. Review on air cathode in Li-air batteries. *J. Technol. Innov. Renew. Energy* **2013**, *2*, 293–305.

99. Martin, J.; Neburchilov, V.; Wang, H.; Qu, W. Air Cathodes for Metal-air Batteries and Fuel Cells. In Proceedings of the 2009 IEEE Electrical Power & Energy Conference (EPEC), Montreal, QC, Canada, 22–23 October 2009; IEEE: Piscataway, NJ, USA, 2009; pp. 1–6.

100. Cai, X.; Lai, L.; Lin, J.; Shen, Z. Recent advances in air electrodes for Zn–air batteries: Electrocatalysis and structural design. *Mater. Horiz.* **2017**, *4*, 945–976. [CrossRef]

101. Lee, C.H.; Lee, S.U. Theoretical basis of electrocatalysis. In *Electrocatalysts for Fuel Cells and Hydrogen Evolution-Theory to Design*; IntechOpen: London, UK, 2018; p. 13.

102. Wang, Z.-L.; Xu, D.; Xu, J.-J.; Zhang, X.-B. Oxygen electrocatalysts in metal–air batteries: From aqueous to nonaqueous electrolytes. *Chem. Soc. Rev.* **2014**, *43*, 7746–7786. [CrossRef]

103. Abdelkareem, M.A.; Sayed, E.T.; Mohamed, H.O.; Obaid, M.; Rezk, H.; Chae, K.-J. Nonprecious anodic catalysts for low-molecular-hydrocarbon fuel cells: Theoretical consideration and current progress. *Prog. Energy Combust. Sci.* **2020**, *77*, 100805. [CrossRef]

104. Al-Dhaifallah, M.; Abdelkareem, M.A.; Rezk, H.; Alhumade, H.; Nassef, A.M.; Olabi, A.G. Co-decorated reduced graphene/titanium nitride composite as an active oxygen reduction reaction catalyst with superior stability. *Int. J. Energy Res.* **2021**, *45*, 1587–1598. [CrossRef]

105. Wang, M.; Fang, Z.; Zhang, K.; Fang, J.; Qin, F.; Zhang, Z.; Li, J.; Liu, Y.; Lai, Y. Synergistically enhanced activity of graphene quantum dots/graphene hydrogel composites: A novel all-carbon hybrid electrocatalyst for metal/air batteries. *Nanoscale* **2016**, *8*, 11398–11402. [CrossRef] [PubMed]

106. Jung, K.-N.; Hwang, S.M.; Park, M.-S.; Kim, K.J.; Kim, J.-G.; Dou, S.X.; Kim, J.H.; Lee, J.-W. One-dimensional manganese-cobalt oxide nanofibres as bi-functional cathode catalysts for rechargeable metal-air batteries. *Sci. Rep.* **2015**, *5*, 7665. [CrossRef]

107. Wang, M.; Lai, Y.; Fang, J.; Qin, F.; Zhang, Z.; Li, J.; Zhang, K. Hydrangea-like $NiCo_2S_4$ hollow microspheres as an advanced bifunctional electrocatalyst for aqueous metal/air batteries. *Catal. Sci. Technol.* **2016**, *6*, 434–437. [CrossRef]

108. Zhao, C.; Yan, X.; Wang, G.; Jin, Y.; Du, X.; Du, W.; Sun, L.; Ji, C. PdCo bimetallic nano-electrocatalyst as effective air-cathode for aqueous metal-air batteries. *Int. J. Hydrogen Energy* **2018**, *43*, 5001–5011. [CrossRef]

109. Zhang, L.; Huang, Q.A.; Yan, W.; Shao, Q.; Zhang, J. Design and fabrication of non-noble metal catalyst-based air-cathodes for metal-air battery. *Can. J. Chem. Eng.* **2019**, *97*, 2984–2993. [CrossRef]

110. Tan, P.; Shyy, W.; Zhao, T.S.; Wei, Z.H.; An, L. Discharge product morphology versus operating temperature in non-aqueous lithium-air batteries. *J. Power Sources* **2015**, *278*, 133–140. [CrossRef]

111. Gilligan, G.; Qu, D. Zinc-air and other types of metal-air batteries. In *Advances in Batteries for Medium and Large-Scale Energy Storage*; Elsevier: Amsterdam, The Netherlands, 2015; pp. 441–461.

112. Han, X.; Li, X.; White, J.; Zhong, C.; Deng, Y.; Hu, W.; Ma, T. Metal–air batteries: From static to flow system. *Adv. Energy Mater.* **2018**, *8*, 1801396. [CrossRef]

113. Liu, W.; Zhang, J.; Bai, Z.; Jiang, G.; Li, M.; Feng, K.; Yang, L.; Ding, Y.; Yu, T.; Chen, Z. Controllable urchin-like $NiCo_2S_4$ microsphere synergized with sulfur-doped graphene as bifunctional catalyst for superior rechargeable Zn–air battery. *Adv. Funct. Mater.* **2018**, *28*, 1706675. [CrossRef]

114. Tran, T.N.T.; Chung, H.-J.; Ivey, D.G. A study of alkaline gel polymer electrolytes for rechargeable zinc–air batteries. *Electrochim. Acta* **2019**, *327*, 135021. [CrossRef]

115. Jacas Biendicho, J.; Noréus, D.; Offer, C.; Svensson, G.; Smith, R.I.; Hull, S. New opportunities for air cathode batteries; in-situ neutron diffraction measurements. *Front. Energy Res.* **2018**, *6*, 69. [CrossRef]

116. Pan, J.; Xu, Y.Y.; Yang, H.; Dong, Z.; Liu, H.; Xia, B.Y. Advanced architectures and relatives of air electrodes in Zn–air batteries. *Adv. Sci.* **2018**, *5*, 1700691. [CrossRef] [PubMed]

117. Ye, L.; Hong, Y.; Liao, M.; Wang, B.; Wei, D.; Peng, H.; Ye, L.; Hong, Y.; Liao, M.; Wang, B.; et al. Recent advances in flexible fiber-shaped metal-air batteries. *Energy Storage Mater.* **2020**, *28*, 364–374. [CrossRef]

118. Xie, Z.; Wu, Z.; An, X.; Yue, X.; Xiaokaiti, P.; Yoshida, A.; Abudula, A.; Guan, G. A sandwich-type composite polymer electrolyte for all-solid-state lithium metal batteries with high areal capacity and cycling stability. *J. Membr. Sci.* **2020**, *596*, 117739. [CrossRef]

119. Qu, S.; Song, Z.; Liu, J.; Li, Y.; Kou, Y.; Ma, C.; Han, X.; Deng, Y.; Zhao, N.; Hu, W.; et al. Electrochemical approach to prepare integrated air electrodes for highly stretchable zinc-air battery array with tunable output voltage and current for wearable electronics. *Nano Energy* **2017**, *39*, 101–110. [CrossRef]

120. Teabnamang, P.; Kao-ian, W.; Nguyen, M.T.; Yonezawa, T.; Cheacharoen, R.; Kheawhom, S. High-Capacity Dual-Electrolyte Aluminum–Air Battery with Circulating Methanol Anolyte. *Energies* **2020**, *13*, 2275. [CrossRef]

121. Cheng, Y.; Li, D.; Shi, L.; Xiang, Z. Efficient unitary oxygen electrode for air-based flow batteries. *Nano Energy* **2018**, *47*, 361–367. [CrossRef]

122. Sun, C.; Negro, E.; Nale, A.; Pagot, G.; Vezzù, K.; Zawodzinski, T.A.; Meda, L.; Gambaro, C.; Di Noto, V. An efficient barrier toward vanadium crossover in redox flow batteries: The bilayer [Nafion/(WO3)x] hybrid inorganic-organic membrane. *Electrochim. Acta* **2021**, *378*, 138133. [CrossRef]

123. Pichler, B.; Berner, B.S.; Rauch, N.; Zelger, C.; Pauling, H.-J.; Gollas, B.; Hacker, V. The impact of operating conditions on component and electrode development for zinc-air flow batteries. *J. Appl. Electrochem.* **2018**, *48*, 1043–1056. [CrossRef]

124. Zhang, H.; Tan, Y.; Luo, X.D.; Sun, C.Y.; Chen, N. Polarization Effects of a Rayon and Polyacrylonitrile Based Graphite Felt for Iron-Chromium Redox Flow Batteries. *ChemElectroChem* **2019**, *6*, 3175–3188. [CrossRef]

125. grosse Austing, J.; Nunes Kirchner, C.; Hammer, E.-M.; Komsiyska, L.; Wittstock, G. Study of an unitised bidirectional vanadium/air redox flow battery comprising a two-layered cathode. *J. Power Sources* **2015**, *273*, 1163–1170. [CrossRef]

126. Wilberforce, T.; Olabi, A.G.; Sayed, E.T.; Elsaid, K.; Abdelkareem, M.A. Progress in carbon capture technologies. *Sci. Total Environ.* **2021**, *761*, 143203. [CrossRef] [PubMed]

127. Abdelkareem, M.A.; Lootah, M.A.; Sayed, E.T.; Wilberforce, T.; Alawadhi, H.; Yousef, B.A.A.; Olabi, A.G. Fuel cells for carbon capture applications. *Sci. Total Environ.* **2021**, *769*, 144243. [CrossRef] [PubMed]

128. Sayed, E.T.; Abdelkareem, M.A.; Alawadhi, H.; Elsaid, K.; Wilberforce, T.; Olabi, A.G. Graphitic carbon nitride/carbon brush composite as a novel anode for yeast-based microbial fuel cells. *Energy* **2021**, *221*, 119849. [CrossRef]

129. Jiao, K.; Xuan, J.; Du, Q.; Bao, Z.; Xie, B.; Wang, B.; Zhao, Y.; Fan, L.; Wang, H.; Hou, Z. Designing the next generation of proton-exchange membrane fuel cells. *Nature* **2021**, *595*, 361–369. [CrossRef]

130. Gittleman, C.S.; Jia, H.; De Castro, E.S.; Chisholm, C.R.; Kim, Y.S. Proton conductors for heavy-duty vehicle fuel cells. *Joule* **2021**, *5*, 1660–1677. [CrossRef]

131. Abdelkareem, M.A.; Elsaid, K.; Wilberforce, T.; Kamil, M.; Sayed, E.T.; Olabi, A. Environmental aspects of fuel cells: A review. *Sci. Total Environ.* **2021**, *752*, 141803. [CrossRef] [PubMed]

132. Wilberforce, T.; Olabi, A.G.; Sayed, E.T.; Elsaid, K.; Maghrabie, H.M.; Abdelkareem, M.A. A review on Zero Energy Buildings–Pros and Cons. *Energy Built Environ.* **2021**. [CrossRef]

133. Maghrabie, H.M.; Elsaid, K.; Sayed, E.T.; Abdelkareem, M.A.; Wilberforce, T.; Olabi, A.G. Building-integrated photovoltaic/thermal (BIPVT) systems: Applications and challenges. *Sustain. Energy Technol. Assess.* **2021**, *45*, 101151.

134. Elavarasan, R.M.; Shafiullah, G.; Padmanaban, S.; Kumar, N.M.; Annam, A.; Vetrichelvan, A.M.; Mihet-Popa, L.; Holm-Nielsen, J.B. A comprehensive review on renewable energy development, challenges, and policies of leading Indian states with an international perspective. *IEEE Access* **2020**, *8*, 74432–74457. [CrossRef]

135. Lu, Y.; Khan, Z.A.; Alvarez-Alvarado, M.S.; Zhang, Y.; Huang, Z.; Imran, M. A critical review of sustainable energy policies for the promotion of renewable energy sources. *Sustainability* **2020**, *12*, 5078. [CrossRef]

136. Adebayo, T.S.; Kirikkaleli, D. Impact of renewable energy consumption, globalization, and technological innovation on environmental degradation in Japan: Application of wavelet tools. *Environ. Dev. Sustain.* **2021**, *23*, 16057–16082. [CrossRef]

137. Rabaia, M.K.H.; Abdelkareem, M.A.; Sayed, E.T.; Elsaid, K.; Chae, K.-J.; Wilberforce, T.; Olabi, A.G. Environmental impacts of solar energy systems: A review. *Sci. Total Environ.* **2021**, *754*, 141989. [CrossRef] [PubMed]

138. Sebestyén, V. Renewable and Sustainable Energy Reviews: Environmental impact networks of renewable energy power plants. *Renew. Sustain. Energy Rev.* **2021**, *151*, 111626. [CrossRef]

139. Mohsin, M.; Kamran, H.W.; Nawaz, M.A.; Hussain, M.S.; Dahri, A.S. Assessing the impact of transition from nonrenewable to renewable energy consumption on economic growth-environmental nexus from developing Asian economies. *J. Environ. Manag.* **2021**, *284*, 111999. [CrossRef]

140. Dincer, I.; Rosen, M.A. *Thermal Energy Storage Systems and Applications*; John Wiley & Sons: Hoboken, NJ, USA, 2021.

141. Lai, C.S.; Locatelli, G. Economic and financial appraisal of novel large-scale energy storage technologies. *Energy* **2021**, *214*, 118954. [CrossRef]

142. Olabi, A.G.; Wilberforce, T.; Elsaid, K.; Sayed, E.T.; Salameh, T.; Abdelkareem, M.A.; Baroutaji, A. A Review on Failure Modes of Wind Turbine Components. *Energies* **2021**, *14*, 5241. [CrossRef]

143. Olabi, A.G.; Wilberforce, T.; Elsaid, K.; Salameh, T.; Sayed, E.T.; Husain, K.S.; Abdelkareem, M.A. Selection Guidelines for Wind Energy Technologies. *Energies* **2021**, *14*, 3244. [CrossRef]

144. Ahmed, S.D.; Al-Ismail, F.S.; Shafiullah, M.; Al-Sulaiman, F.A.; El-Amin, I.M. Grid integration challenges of wind energy: A review. *IEEE Access* **2020**, *8*, 10857–10878. [CrossRef]

145. Nazir, M.S.; Ali, N.; Bilal, M.; Iqbal, H.M. Potential environmental impacts of wind energy development: A global perspective. *Curr. Opin. Environ. Sci. Health* **2020**, *13*, 85–90. [CrossRef]

146. Iqbal, A.; Mahmoud, M.S.; Sayed, E.T.; Elsaid, K.; Abdelkareem, M.A.; Alawadhi, H.; Olabi, A.G. Evaluation of the nanofluid-assisted desalination through solar stills in the last decade. *J. Environ. Manag.* **2021**, *277*, 111415. [CrossRef] [PubMed]

147. Maghrabie, H.M.; Abdelkareem, M.A.; Al-Alami, A.H.; Ramadan, M.; Mushtaha, E.; Wilberforce, T.; Olabi, A.G. State-of-the-Art Technologies for Building-Integrated Photovoltaic Systems. *Buildings* **2021**, *11*, 383. [CrossRef]

148. Zhang, Y.; Ren, J.; Pu, Y.; Wang, P. Solar energy potential assessment: A framework to integrate geographic, technological, and economic indices for a potential analysis. *Renew. Energy* **2020**, *149*, 577–586. [CrossRef]

149. Irfan, M.; Elavarasan, R.M.; Hao, Y.; Feng, M.; Sailan, D. An assessment of consumers' willingness to utilize solar energy in China: End-users' perspective. *J. Clean. Prod.* **2021**, *292*, 126008. [CrossRef]

150. Fan, X.; Liu, B.; Liu, J.; Ding, J.; Han, X.; Deng, Y.; Lv, X.; Xie, Y.; Chen, B.; Hu, W.; et al. Battery technologies for grid-level large-scale electrical energy storage. *Trans. Tianjin Univ.* **2020**, *26*, 92–103. [CrossRef]

151. Salameh, T.; Sayed, E.T.; Abdelkareem, M.A.; Olabi, A.G.; Rezk, H. Optimal selection and management of hybrid renewable energy System: Neom city as a case study. *Energy Convers. Manag.* **2021**, *244*, 114434. [CrossRef]

152. Shinde, P.A.; Chodankar, N.R.; Abdelkareem, M.A.; Han, Y.-K.; Olabi, A.G. Nitridation-induced in situ coupling of Ni-Co4N particles in nitrogen-doped carbon nanosheets for hybrid supercapacitors. *Chem. Eng. J.* **2022**, *428*, 131888. [CrossRef]

153. Hameer, S.; van Niekerk, J.L. A review of large-scale electrical energy storage. *Int. J. Energy Res.* **2015**, *39*, 1179–1195. [CrossRef]

154. Liu, Y.; Sun, Q.; Li, W.; Adair, K.R.; Li, J.; Sun, X. A comprehensive review on recent progress in aluminum–air batteries. *Green Energy Environ.* **2017**, *2*, 246–277. [CrossRef]

155. Sayed, E.T.; Shehata, N.; Abdelkareem, M.A.; Atieh, M.A. Recent progress in environmentally friendly bio-electrochemical devices for simultaneous water desalination and wastewater treatment. *Sci. Total Environ.* **2020**, *748*, 141046. [CrossRef] [PubMed]

156. Srimuk, P.; Wang, L.; Budak, Ö.; Presser, V. High-performance ion removal via zinc–air desalination. *Electrochem. Commun.* **2020**, *115*, 106713. [CrossRef]

157. Sayed, E.T.; Al Radi, M.; Ahmad, A.; Abdelkareem, M.A.; Alawadhi, H.; Atieh, M.A.; Olabi, A.G. Faradic capacitive deionization (FCDI) for desalination and ion removal from wastewater. *Chemosphere* **2021**, *275*, 130001. [CrossRef] [PubMed]
158. Al Radi, M.; Sayed, E.T.; Alawadhi, H.; Abdelkareem, M.A. Progress in energy recovery and graphene usage in capacitive deionization. *Crit. Rev. Environ. Sci. Technol.* **2021**, 1–57. [CrossRef]
159. Ghahari, M.; Rashid-Nadimi, S.; Bemana, H. Metal-air desalination battery: Concurrent energy generation and water desalination. *J. Power Sources* **2019**, *412*, 197–203. [CrossRef]
160. Ghahari, M.; Nadimi, S.R. Integration of metal-air batteries with electrodialysis system to decrease of required energy for water desalination. In Proceedings of the 23rd Iranian Seminar of Analytical Chemistry, Tehran, Iran, 30 August–1 September 2016.
161. Zhao, C.; Liu, G.; Sun, N.; Zhang, X.; Wang, G.; Zhang, Y.; Zhang, H.; Zhao, H. Biomass-derived N-doped porous carbon as electrode materials for Zn-air battery powered capacitive deionization. *Chem. Eng. J.* **2018**, *334*, 1270–1280. [CrossRef]
162. Sun, Y.; Liu, X.; Jiang, Y.; Li, J.; Ding, J.; Hu, W.; Zhong, C. Recent advances and challenges in divalent and multivalent metal electrodes for metal–air batteries. *J. Mater. Chem. A* **2019**, *7*, 18183–18208. [CrossRef]